BIOCHEMISTRY

Activation of atypical protein kinase C by sphingosine 1-phosphate revealed by an aPKC-specific activity reporter

Taketoshi Kajimoto[1,2]*, Alisha D. Caliman[1], Irene S. Tobias[1], Taro Okada[2], Caila A. Pilo[1], An-Angela N. Van[1], J. Andrew McCammon[1], Shun-ichi Nakamura[2], Alexandra C. Newton[1]*

Atypical protein kinase C (aPKC) isozymes are unique in the PKC superfamily in that they are not regulated by the lipid second messenger diacylglycerol, which has led to speculation about whether a different second messenger acutely controls their function. Here, using a genetically encoded reporter that we designed, aPKC-specific C kinase activity reporter (aCKAR), we found that the lipid mediator sphingosine 1-phosphate (S1P) promoted the cellular activity of aPKC. Intracellular S1P directly bound to the purified kinase domain of aPKC and relieved autoinhibitory constraints, thereby activating the kinase. In silico studies identified potential binding sites on the kinase domain, one of which was validated biochemically. In HeLa cells, S1P-dependent activation of aPKC suppressed apoptosis. Together, our findings identify a previously undescribed molecular mechanism of aPKC regulation, a molecular target for S1P in cell survival regulation, and a tool to further explore the biochemical and biological functions of aPKC.

INTRODUCTION

The atypical protein kinase C (aPKC) class consists of two isozymes, PKCζ and PKCι/λ (PKCλ is the mouse ortholog of human PKCι). In addition, the gene encoding PKCζ also encodes an N-terminally truncated form called PKMζ, which is constitutively active. The aPKC isozymes are involved in diverse cellular functions, including a well-characterized role in the maintenance of cell polarity and insulin signaling (1, 2). They have also been extensively studied in cancer, wherein these isozymes can function as either oncogenes or tumor suppressors depending on the cellular context (3–5). In particular, the gene encoding PKCι (PRKCI) is part of the 3q amplicon, a highly amplified region that includes oncogenes such as that encoding phosphoinositide 3-kinase (PI3K) (6); thus, the expression of PKCι is increased in many cancers (5). Unlike other PKC family members, aPKC isozymes do not transduce signals resulting from phospholipid hydrolysis (7). Rather, they are activated by binding protein scaffolds. Whether their activity is also acutely activated by second messengers remains to be established.

aPKC isozymes are cotranslationally phosphorylated by mammalian target of rapamycin complex 2 on the turn motif, followed by posttranslational and constitutive phosphorylation by phosphoinositide-dependent protein kinase-1 on the activation loop, modifications that are required for activity (8, 9). As with other PKC family members, the phosphorylated enzymes are maintained in an autoinhibited conformation through the interaction of a pseudosubstrate-C1 domain module with the kinase domain. Binding to protein scaffolds not only positions these PKC isozymes near their substrates but also relieves autoinhibitory constraints by tethering the pseudosubstrate away from the substrate-binding cavity (1). For example, the interaction of PKCζ with the scaffolding protein p62 results in the tethering of the basic PKCζ pseudosubstrate to an acidic surface of the PB1 (Phox-Bem1)

domain of p62, stabilizing the open and active conformation of the kinase (10). Similarly, PKCζ is maintained in an open conformation when bound to the cell polarity–associated protein Par6 (11, 12). One of the effects of insulin is to induce the interaction of aPKC isozymes with protein scaffolds, such as insulin receptor substrate-1 (12). Co-localization of aPKC isozymes and substrates on protein scaffolds ensures efficient phosphorylation given the exceptionally slow catalytic rate of these isozymes, which is 40-fold slower compared to that of conventional PKC isozymes (9). Although aPKC isozymes are not regulated by diacylglycerol, several lines of evidence suggest that other lipid mediators may regulate the activity of aPKC isozymes. In addition to anionic lipids, the neutral lipid ceramide has been reported to directly activate aPKC in vitro (13–16). Ceramide is at the hub of sphingolipid metabolism, involving a network of bioactive lipids that are key regulators of survival and metabolic signaling (17) and pose as attractive second messenger candidates for regulation of aPKC in cells.

Sphingosine 1-phosphate (S1P) has been implicated as an important lipid mediator acting both inside and outside the cell (18–22). It is produced intracellularly by sphingosine kinase (SphK)–catalyzed phosphorylation of sphingosine (Sph) and is then exported out of cells, where it binds heterotrimeric GTP-binding protein–coupled S1P receptors (S1P$_{1–5}$) to regulate a variety of cellular functions. These receptors mediate proinflammatory and prosurvival signaling (23–25). In addition, mounting evidence supports a role for intracellular S1P in cell signaling (17). However, less is known about the molecular mechanisms of its intracellular second messenger function. It has been reported to bind and modulate the activity of signaling molecules such as histone deacetylase, tumor necrosis factor (TNF) receptor–associated factor 2 (TRAF2), and human telomerase reverse transcriptase (26–28). Whether S1P has additional targets is not currently known. Because aberrant sphingolipid signaling is associated with multiple pathologies, including cancer, metabolic disorders, and neurodegeneration (19), identifying the mechanisms and targets of S1P has important therapeutic potential.

[1]Department of Pharmacology, University of California at San Diego, La Jolla, CA 92037, USA. [2]Division of Biochemistry, Department of Biochemistry and Molecular Biology, Graduate School of Medicine, Kobe University, Kobe 650-0017, Japan.
*Corresponding author. Email: anewton@ucsd.edu (A.C.N.); tkajimot@med.kobe-u.ac.jp (T.K.)

Here, we found that intracellular S1P directly binds and activates aPKC isozymes. As part of this study, we developed a genetically encoded reporter specific for aPKC isozymes that enabled us to assess the activity of aPKC in real time in cells. A combination of computational, biochemical, and imaging technologies revealed that S1P bound a pocket on the surface of the kinase domain, reducing autoinhibitory contacts with the pseudosubstrate-C1 module to cause activation. Cellular studies further revealed that basal S1P promoted activation of aPKC and that this basal activity inhibited apoptosis. Our results suggest that S1P allosterically activates aPKC isozymes to suppress apoptosis.

RESULTS

### Modification of C kinase activity reporter creates an aPKC reporter

To examine the activity of aPKC in cells, we modified the phospho-acceptor sequence in our C kinase activity reporter (CKAR) (29) to be uniquely phosphorylated by aPKC. CKAR contains a phospho-threonine (Thr)–binding FHA2 domain and a peptide sequence that conforms to an FHA2-binding sequence when phosphorylated [specifically having a Thr at the phosphoacceptor site and Ile at the P+3 position (30)], flanked by the fluorescence resonance energy transfer (FRET) pair cyan fluorescent protein (CFP) and yellow fluorescent protein (YFP) (Fig. 1A). Phosphorylation at the phospho-acceptor site results in an intramolecular association with the FHA2 module, detected by a decrease in intramolecular FRET. In the original CKAR, this sequence is RFRRFQTLKIKAKA, where the underlined residue is the phosphoacceptor site. We previously modified this sequence to selectively monitor the activity of PKCδ by inserting a phosphorylation sequence that we optimized for this isozyme (31). Here, we took advantage of aPKC's specific phosphorylation of insulin-regulated membrane aminopeptidase (IRAP) at Ser^{80} (32) but made two modifications to conform to the FHA2 consensus sequence: Ser at the phosphoacceptor site was replaced with Thr, and the residue at the P+3 position was replaced with Ile (Fig. 1A). To determine whether aPKC-specific CKAR (aCKAR) is phosphorylated by endogenous or overexpressed aPKC isozymes in cells, COS7 cells were transfected with aCKAR and either mCherry or the constitutively active catalytic domain of PKCζ (PKMζ; tagged at the N terminus with mCherry) and then treated with the aPKC-specific inhibitor PZ09 (33). Inhibition of aPKC resulted in a small but reproducible drop in FRET ratio (Fig. 1B). The inhibitor-induced drop in the FRET ratio reflects a reduction in the basal phosphorylation of the reporter by aPKC. Thus, the reporter was sensitive to inhibition of both endogenous aPKC isozymes (Fig. 1B, blue) and overexpressed PKMζ (red). For comparison, the FRET ratio change measured by the original CKAR was 1.7× greater for endogenous aPKC activity and 2.9× greater for overexpressed PKMζ (Fig. 1B, blue and red, respectively; compare left and right panels). Thus, aPKC-specific phosphorylation results in a lower magnitude change of aCKAR compared to the generic CKAR. Note that both aCKAR and CKAR have a similar dynamic range, but increased phosphatase sensitivity of aCKAR results in smaller FRET ratio changes upon PZ09 addition; calyculin treatment to inhibit phosphatases results in a much larger change in FRET ratio of aCKAR compared to CKAR in cells overexpressing the constitutively active PKMζ (fig. S1). Qualitatively similar results were obtained for the corresponding catalytic domain–only construct of PKCλ (Fig. 1C). To determine whether

aCKAR can be phosphorylated by other PKC isozymes, COS7 cells transfected with aCKAR were treated with phorbol 12,13-dibutyrate (PDBu) to induce maximal activity of all conventional (α, βII, and γ) and novel (δ, ε, η, and θ) PKC isozymes (Fig. 1D, left). PDBu did not cause an increase in aCKAR readout for cells cotransfected with mCherry alone (measuring endogenous PKC responses) nor did it increase substantially in cells cotransfected with PKCα (Fig. 1D, left, red), PKCβII (yellow), PKCδ (green), or PKCε (pink). In contrast, a robust increase in FRET ratio was observed when the reporter was CKAR (Fig. 1D, right). Thus, aCKAR specifically reads out the activity of PKCζ and PKCι/λ and is not phosphorylated upon activation of phorbol ester–sensitive PKC isozymes. To further validate that the inhibitor-sensitive activity was catalyzed by aPKC, we examined PZ09-sensitive activity in cells in which both PKCζ and PKCι/λ had been depleted by small interfering RNAs (siRNA). The knockdown of PKCζ was largely efficient, whereas as that of PKCι was by about half (Fig. 1E). Depletion of both aPKC isozymes resulted in a robust reduction in basal activity, as assessed by the much smaller drop in reporter readout in cells treated with siRNA to both isozymes (Fig. 1F, red) compared to control cells (Fig. 1F, blue). In addition, replacement of the phosphoacceptor Thr with Ala abolished the change in FRET ratio observed upon inhibition of endogenous aPKC (Fig. 1G, yellow) or overexpressed PKMζ (Fig. 1G, green). Furthermore, aCKAR showed no response to stimulation of COS7 cells with forskolin to increase the abundance of cyclic adenosine monophosphate (cAMP) under conditions that resulted in a robust response by the A kinase activity reporter (AKAR) (Fig. 1H) (34). Similarly, stimulation of the cells with epidermal growth factor (EGF) did not cause a change in aCKAR readout under conditions where a robust response was seen from the AKT [also known as protein kinase B (PKB); hereafter, referred to as AKT/PKB] activity reporter BKAR (B kinase activity reporter) (Fig. 1I) (35). In addition, treatment with PDBu resulted in no change under conditions where a similarly large response was seen from the D kinase activity reporter (DKAR) (Fig. 1J) (36). These data reveal that aCKAR reads out the basal activity of endogenous aPKC isozymes and the basal activity of the overexpressed catalytic domain of PKCζ and PKCι/λ but does not read out the activity of conventional PKC isozymes, novel PKC isozymes, PKA, PKB, or PKD.

Having validated that aCKAR is appropriate to specifically monitor endogenous aPKC signaling in cells, we interrogated the endogenous signaling output of aPKC isozymes in a diverse set of cell types. Treatment with PZ09 caused a drop in aCKAR readout in all cells examined, including COS7, human embryonic kidney (HEK) 293, HeLa, HepG2, MCF7, MDA-MB-231, and SH-SY5Y (Fig. 2A). Quantification of the FRET ratio change observed in the period of 10 to 12 min after inhibitor treatment revealed that the breast cancer cell line MDA-MB-231 had the highest basal signaling output of aPKC isozymes (Fig. 2B). The lowest basal signaling was observed in the liver cell line HepG2, the fibroblast cell line HEK293, and the neuro-blastoma cell line SH-SY5Y, where the FRET ratio changes were about threefold lower than that for the MDA-MB-231 cell line. Western blot analysis of equal numbers for each cell type revealed that all cells expressed both PKCζ and PKCι (Fig. 2C; immunoreactivity for PKCζ and PKCι quantified in Fig. 2D, respectively). Cells with the highest amounts of aPKC activity did not necessarily have the highest abundance of PKCζ and/or PKCι protein; for example, MDA-MB-231 cells had high basal aPKC signaling but relatively low abundance of

Fig. 1. Development of an aPKC-selective activity reporter. (**A**) The architecture of aCKAR is based on that of the pan-PKC reporter CKAR and consists of monomeric CFP (cyan), the FHA2 domain of Rad53p (blue), an aPKC-selective substrate peptide (red), and monomeric YFP (yellow). In the unphosphorylated state, monomeric CFP and monomeric YFP are in proximity and in an orientation resulting in FRET. Once phosphorylated by aPKC at the Thr within the substrate sequence (highlighted in yellow), the FHA2 domain binds the phosphorylated sequence, resulting in a conformational change that alters the FRET ratio. Ile at the P+3 position (highlighted in green) is critical for the binding of phospho-Thr to the FHA2 domain. The substrate peptide of CKAR was replaced with an aPKC-selective substrate peptide with a sequence corresponding to residues 74 to 87 of IRAP [rat IRAP (U76997)], except Ser[80] at the phosphoacceptor site was replaced with Thr (yellow) and the Asn at the P+3 position was replaced with Ile (green). (**B**) COS7 cells were cotransfected with aCKAR (left) or CKAR (right) and mCherry (Vector) or mCherry-PKMζ. The CFP/YFP FRET (C/Y) emission ratio was quantified as a
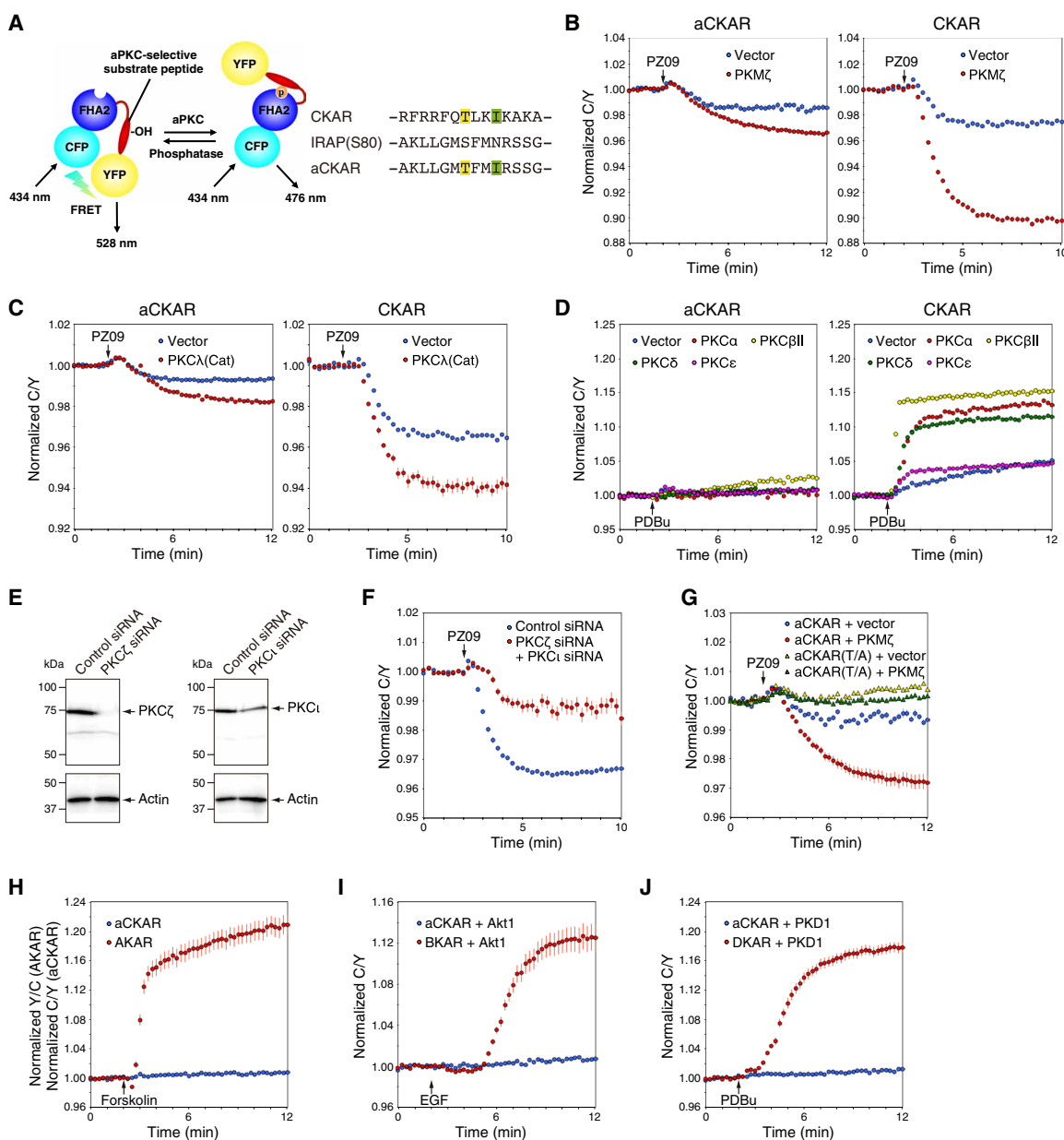
function of time after the addition of PZ09 (5 μM). The drop in FRET ratio upon addition of inhibitor represents the basal (unstimulated) activity of endogenous aPKC (blue); the additional drop in cells overexpressing PKMζ (red) reflects the basal activity of PKMζ. Data are mean (± SE) C/Y emission ratios normalized to the starting point (1.0) from $n \geq 25$ cells. (**C**) As in (B), except that cells were cotransfected with the indicated reporters and either red fluorescent protein (RFP) or RFP tagged to a construct of the catalytic domain of PKCλ [PKCλ(Cat)]. Data are means ± SE from $n \geq 21$ cells. (**D**) COS7 cells were cotransfected with aCKAR (left) or CKAR (right) and mCherry, mCherry-PKCα, mCherry-PKCβII, mCherry-PKCδ, or mCherry-PKCε. The normalized C/Y emission ratio was quantified as a function of time after the addition of PDBu (200 nM). The increase in FRET ratio represents the agonist-induced activity of these PKC isozymes. Data are means ± SE from $n \geq 16$ cells (left) or ≥ 21 cells (right). (**E**) Knockdown of endogenous expression of PKCζ and PKCι in HeLa cells using siRNAs for human PKCζ and PKCι. HeLa cells were transfected for 48 hours with non-targeting control siRNA, human PKCζ siRNA, or human PKCι siRNA individually. Equal aliquots of lysate were blotted and probed with antibodies against PKCζ, PKCι, and actin (protein loading control). (**F**) HeLa cells were cotransfected with aCKAR and control siRNA or both PKCζ siRNA and PKCι siRNA. The normalized C/Y emission ratio was quantified as a function of time after the addition of PZ09 (5 μM). Data represent the means ± SE from $n \geq 21$ cells. (**G**) COS7 cells were cotransfected with aCKAR or a construct in which the phosphoacceptor site is mutated to Ala [aCKAR(T/A)] and mCherry or mCherry-PKMζ. The normalized C/Y emission ratio was quantified as a function of time after the addition of PZ09 (5 μM). Data are means ± SE from $n \geq 28$ cells. (**H**) COS7 cells were transfected with aCKAR or the PKA reporter AKAR. The normalized C/Y emission ratio was quantified as a function of time after the addition of forskolin (10 μM) to increase the production of cAMP. Data are means ± SE from $n \geq 28$ cells. (**I**) COS7 cells were cotransfected with aCKAR or the AKT/PKB reporter BKAR and mCherry-Akt1. The normalized C/Y emission ratio was quantified as a function of time after the addition of EGF (50 ng/ml) to activate AKT/PKB. Data are means ± SE from $n \geq 28$ cells. (**J**) COS7 cells were cotransfected with aCKAR or the PKD reporter DKAR and mCherry-PKD1. The normalized C/Y emission ratio was quantified as a function of time after the addition of PDBu (200 nM) to activate PKD (and PKC, which does not phosphorylate this reporter). Data are means ± SE from $n \geq 25$ cells.
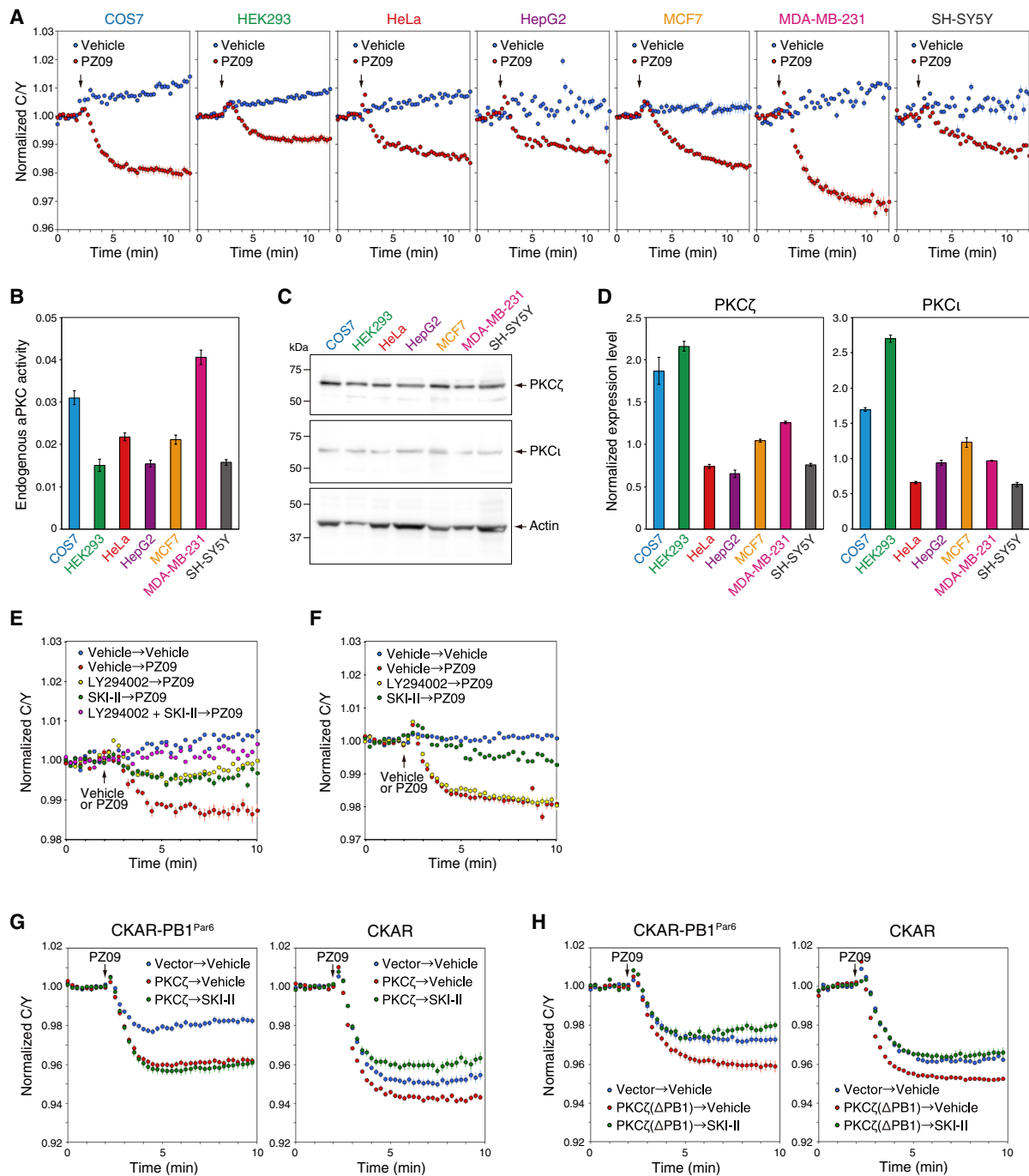
Fig. 2. Basal activity of aPKC is regulated by S1P signaling. (**A**) COS7, HEK293, HeLa, HepG2, MCF7, MDA-MB-231, or SH-SY5Y cells were transfected with aCKAR. The basal activity of endogenous aPKC was measured after the addition of PZ09 (5 μM); dimethyl sulfoxide (DMSO) vehicle was added as a control. The normalized C/Y emission ratio was quantified as a function of time after the addition of PZ09. Data are means ± SE from $n \geq 20$ cells. The arrow indicates the point of DMSO vehicle or PZ09 addition. (**B**) The relative basal activity of endogenous aPKC was quantified from the data in (A) and represents the difference between the C/Y emission ratios summed between 10 and 12 min for the vehicle versus PZ09 treatments. (**C**) Western blot of lysates from 2.0×10^5 cells of the indicated cell lines probed with antibodies to PKCζ or PKCι. The endogenous abundance of β-actin was also detected using an anti–β-actin antibody. (**D**) Normalized abundance of PKCζ (left) or PKCι (right) was quantified from the result of (C) and represents the intensity of PKC divided by the intensity of β-actin for each cell type. (**E**) HeLa cells were transfected with aCKAR and pretreated for 16 hours with DMSO vehicle, LY294002 (20 μM), SKI-II (5 μM), or LY294002 (20 μM) + SKI-II (5 μM). These cells were subsequently ("→" in graph legend) stimulated with DMSO vehicle or 5 μM PZ09 (addition indicated by vertical arrow) to assess the effect of these pretreatments on basal aPKC activity. The normalized C/Y emission ratio was quantified as a function of time. Data are means ± SE from $n \geq 22$ cells. (**F**) As in (E), except experiments were conducted in serum-free media. Data are means ± SE from $n \geq 22$ cells. (**G**) HeLa cells were cotransfected with CKAR fused to the PB1 domain of Par6 (CKAR-PB1^Par6; left) or CKAR (right) and mCherry (Vector) or mCherry-PKCζ (PKCζ). Cells were pretreated with DMSO vehicle or SKI-II (5 μM) for 16 hours and then treated with PZ09 (5 μM). The normalized C/Y emission ratio was quantified as a function of time. Data are means ± SE from $n \geq 22$ cells. (**H**) As in (G), except cells were transfected with mCherry-PKCζ (PB1 deletion mutant) [PKCζ(ΔPB1)] where indicated. Data are means ± SE from $n \geq 17$ cells.

aPKC protein. HeLa cells also had low protein abundance of aPKC isozymes but moderate basal aPKC activity. We selected HeLa cells for subsequent experiments, reasoning that moderate basal activity might enable easier detection of both basal and agonist-stimulated activity.

S1P contributes to the basal activity of nonscaffolded aPKC
We used a pharmacological approach to address whether the basal activity of aPKC is regulated by S1P. As noted above, treatment of aCKAR-overexpressing HeLa cells with PZ09 in the presence of serum caused a drop in FRET ratio that represents the inhibition of basally active aPKC isozymes (Fig. 2E). Pretreatment of HeLa cells either with the SphK inhibitor SKI-II (Fig. 2E, green) to reduce the amount of intracellular S1P (37), or the PI3K inhibitor LY294002 (yellow) to reduce phosphatidylinositol 3,4,5-trisphosphate abundance, resulted in a twofold smaller drop in FRET ratio change upon PZ09 treatment. Pretreatment with both inhibitors (Fig. 2E, pink) abolished all basal activity as assessed by the lack of substantial change in FRET ratio upon addition of PZ09. In contrast, the PI3K inhibitor had no effect on the activity of endogenous aPKC in serum-starved cells (Fig. 2F, yellow). Under these conditions, the SphK inhibitor abolished almost all endogenous aPKC activity (green). These data reveal that S1P stimulates the activity of endogenous aPKC isozymes in HeLa cells by a mechanism independent of serum growth conditions.

Binding to protein scaffolds such as Par6 displaces the pseudosubstrate segment of aPKC isozymes, leading us to ask whether scaffold-activated aPKC was sensitive to S1P. CKAR fused to the PB1 domain of Par6 (CKAR-PB1^{Par6}) displayed robust sensitivity to treatment of cells with PZ09 (Fig. 2G, left, red), reflecting the high basal activity of aPKC on this scaffold (10, 12). The basal activity on the scaffold was twofold greater than that read out by the cytosolic reporter (CKAR; compare blue). aPKC activity measured on the Par6 scaffold using CKAR-PB1^{Par6} was insensitive to inhibition of SphK (green circles). A similar result was obtained in MCF7 and MDA-MB-231 cells (fig. S2). Deletion of the PB1 domain of PKCζ to prevent binding to the Par6 scaffold restored S1P sensitivity to activity readout by CKAR-PB1^{Par6} (Fig. 2H). These data reveal that aPKC bound to Par6 is not sensitive to S1P, contrasting with the sensitivity of cytosolic aPKC to S1P.

Intracellular S1P mediates cellular activation of aPKC
To confirm that the SKI-II–dependent inhibition of aPKC activity was a result of depleting intracellular S1P, we tested whether this inhibition could be rescued by acute release of S1P from photolysis of caged S1P. Addition of PZ09 to HeLa cells caused the characteristic ~3% drop in FRET ratio (Fig. 3A, red); this FRET ratio change was about 10-fold lower when cells were pretreated with SKI-II overnight (Fig. 3A, yellow). This PZ09-dependent change in FRET ratio for the SKI-II–treated cells could be restored to that seen in the controls (non–SKI-II pretreatment) if cells were loaded with caged S1P (38, 39) and then exposed to ultraviolet (UV) light for 5 min to uncage the lipid (Fig. 3A, pink). This rescue of caged S1P–loaded cells was not observed in cells loaded with caged S1P that were not exposed to UV light (Fig. 3A, green). To further validate that the basal activity of aPKC results from S1P generated by SphK, we knocked down SphK1 or SphK2 by siRNA; analysis of mRNA revealed about a 50% knockdown of each (Fig. 3B). Knockdown of either SphK1 or SphK2 (Fig. 3C, red and yellow, respectively) caused a modest re-

duction in basal activity compared to that of control cells (blue), whereas knockdown of both SphK1 and SphK2 (green) caused a greater than 80% reduction in basal activity relative to that of controls. Lastly, addition of caged S1P to the double-knockdown cells resulted in a robust increase in basal activity, similar to that for control cells (Fig. 3D, red), after photolysis to uncage S1P (pink); no effect was observed in the absence of photolysis (green). These data demonstrate that S1P is necessary and sufficient for the basal activity of aPKC observed in this study. In addition, knockdown and inhibitor studies are consistent with basally active SphK generating S1P to basally activate aPKC.

We next asked whether the basally active aPKC could be further stimulated upon addition of S1P. Uncaging of S1P in HeLa cells loaded with caged S1P resulted in an increase in aPKC activity (Fig. 3E, red) relative to cells that had not been loaded with the caged lipid (Fig. 3E, blue). This increase was reversed by addition of PZ09, revealing that addition of S1P induced the aPKC-dependent phosphorylation of aCKAR. To address whether extracellular S1P could also activate aPKC isozymes, we first determined which S1P receptors are expressed in HeLa cells to target them pharmacologically. qPCR analysis established that the major S1P receptor in HeLa cells is S1P$_1$, with relatively low amounts of S1P$_3$ and no substantial amounts of S1P$_2$, S1P$_4$, and S1P$_5$ (Fig. 3F). Treatment with a high concentration of S1P increases the abundance of total intracellular pools of S1P (26). Treatment of cells with a relatively high concentration of extracellular S1P (10 μM), but not with a low, physiologically relevant concentration (100 nM), caused an increase in aPKC activity (Fig. 3G). This increase was not affected by cotreatment with a selective antagonist of the S1P$_1$ and S1P$_3$ receptors, VPC23019 (Fig. 3G, green). Thus, the activation of aPKC by high concentrations of exogenously added S1P was independent of S1P receptor signaling and likely reflects accumulation of the lipid intracellularly. Together, these data reveal that aPKC is activated by intracellular, but not receptor-dependent extracellular, S1P.

S1P directly binds and activates aPKC
To gain insight into the mechanism by which intracellular S1P activates aPKC, we purified PKCζ to homogeneity and determined whether S1P stimulated its activity using an in vitro kinase assay. Addition of 30 μM S1P increased the rate of phosphorylation of myelin basic protein (MBP), a reaction that was linear up to 25 min (Fig. 4A). Addition of increasing concentrations of S1P revealed dose-dependent activation, with 30 μM S1P doubling the rate of substrate phosphorylation (Fig. 4B). This activation by S1P was reduced by PZ09 (10 μM; Fig. 4C); was not sensitive to acyl chain unsaturation, given that dihydro-S1P (DH-S1P) also activated the enzyme (Fig. 4D); and was specific for the phosphate group of S1P, given that Sph did not alter the activity of PKCζ (Fig. 4E). To address the effect of S1P on the canonical phosphatidylserine (PS) dependence of aPKC activation, we assessed the effect of trace S1P on the concentration of PS resulting in half-maximal activation of PKCζ using the well-characterized Triton X-100/lipid mixed micelle assay (40, 41). The presence of 5 mole percent (mol %) S1P reduced the concentration of PS resulting in half-maximal activity (from 6.5 ± 0.8 mol % to 0.49 ± 0.01 mol %) but did not affect the V_{max} at saturating PS. This low concentration of S1P was also sufficient to double the basal activity in the absence of PS (Fig. 4F). Consistent with the micelle data, the activation of PKCζ by PS in lipid bilayers (9, 42) was not further enhanced by

S1P (Fig. 4G). These results are suggestive of S1P binding to aPKC and releasing autoinhibitory constraints. If this hypothesis is correct, we reasoned that the isolated kinase domain of PKCζ, PKMζ, should be insensitive to activation by S1P. SKI-II treatment had no effect on the PZ09-dependent inhibition of PKMζ activity compared to its effect on untreated cells (Fig. 4H, green and yellow triangles, respectively). In contrast, SKI-II reduced the PZ09-dependent inhibition of wild-type PKCζ compared to vehicle-treated cells (Fig. 4H, red and blue circles, respectively). These data suggest that S1P facilitates the activation of S1P by removing autoinhibitory constraints.

We next tested whether S1P directly binds to PKC. We developed a new assay to monitor the binding of nitrobenzoxadiazole (NBD)–labeled S1P to PKC using flow cytometry to detect protein with bound fluorescent lipid. Binding of NBD-S1P was detected on PKCδ and PKCζ but not PKCα or PKCγ (Fig. 5A). We next measured the binding of (unmodified) S1P to aPKC using a protein-lipid overlay (PLO) assay. The S1P-PKCζ binding was dose dependent, with

300 pmol of S1P resulting in maximal binding to PKCζ (500 ng/ml; Fig. 5B). As a control, we detected comparable S1P binding to the RING domain of TRAF2, a known S1P-binding protein (Fig. 5C) (26). Binding was specific for the Sph backbone because Sph also bound, but no binding by lysophosphatidic acid (LPA) was detected (Fig. 5D). Intermediate binding was observed with both ceramide and PS, known binding lipids for aPKC (Fig. 5D) (13, 15, 43). Last, various domain-deletion mutants of PKCζ were purified (Fig. 5E), and their S1P binding was examined. S1P bound to all constructs that contained the kinase domain: wild-type (i.e., full length), one deleted in the PB1 domain (ΔPB1), one deleted in the pseudosubstrate (ΔPseudo), one deleted in the C1 domain (ΔC1), one deleted in the PDZ ligand (ΔPDZ), and one deleted in the regulatory moiety (ΔReg) (Fig. 5F). However, binding of S1P to a construct in which the kinase domain was deleted (ΔCat) was not observed (Fig. 5F, right). These data suggest that S1P binds the kinase domain of PKCζ.

We next set out to identify whether there is a specific binding pocket for S1P on the surface of the aPKC kinase domain by a strategy
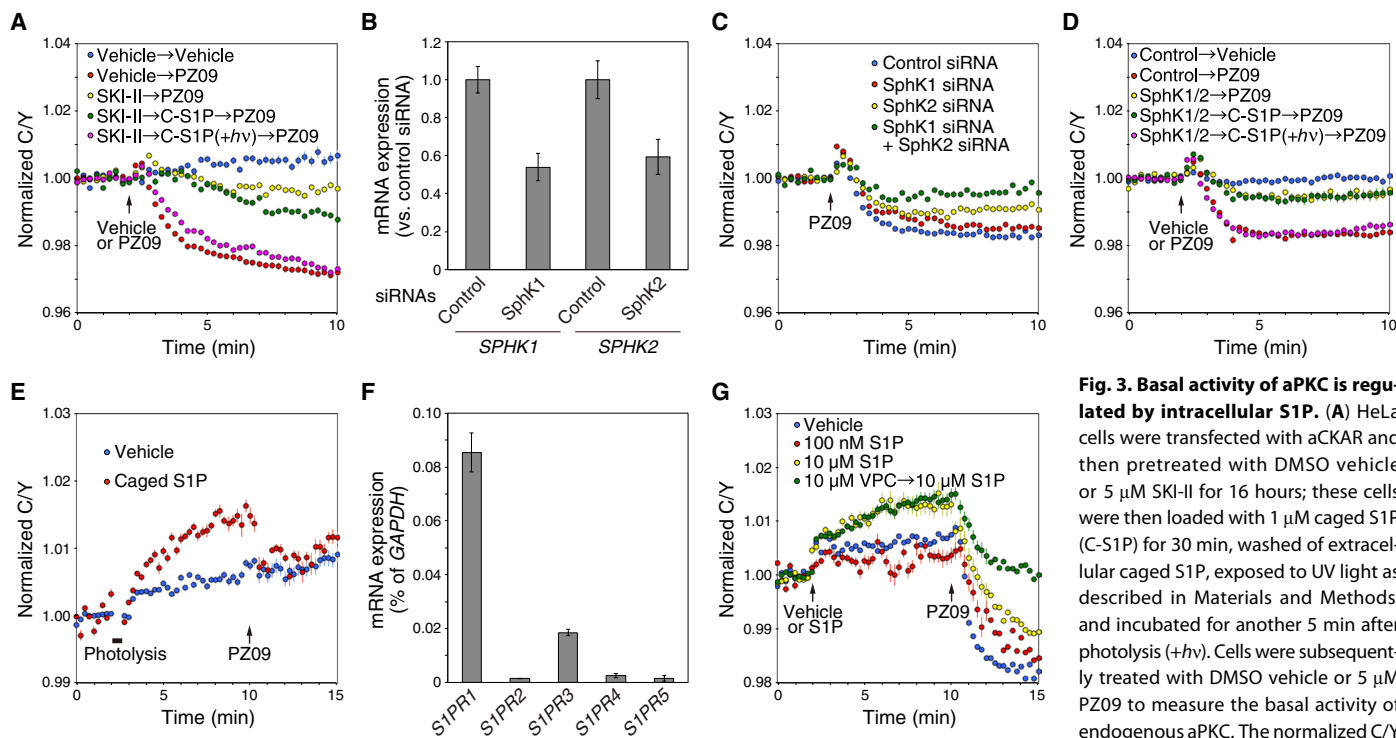
Fig. 3. Basal activity of aPKC is regulated by intracellular S1P. (**A**) HeLa cells were transfected with aCKAR and then pretreated with DMSO vehicle or 5 μM SKI-II for 16 hours; these cells were then loaded with 1 μM caged S1P (C-S1P) for 30 min, washed of extracellular caged S1P, exposed to UV light as described in Materials and Methods, and incubated for another 5 min after photolysis (+hν). Cells were subsequently treated with DMSO vehicle or 5 μM PZ09 to measure the basal activity of endogenous aPKC. The normalized C/Y emission ratio was quantified as a function of time after DMSO vehicle or PZ09 treatment. Data are means ± SE from n ≥ 27 cells. The arrow indicates the point of DMSO vehicle or PZ09 addition. (**B**) Knockdown of endogenous expression of SphK1 and SphK2 in HeLa cells using siRNAs for human SphK1 and SphK2. HeLa cells were transfected for 48 hours with nontargeting control siRNA, human SphK1 siRNA, or human SphK2 siRNA individually. Relative mRNA expression of *SPHK1* and *SPHK2* in HeLa cells were analyzed by real-time quantitative polymerase chain reaction (RT-qPCR). Data are means ± SE from at least three independent experiments. (**C**) HeLa cells were cotransfected with aCKAR and control siRNA, SphK1 siRNA, SphK2 siRNA, or both SphK1 siRNA and SphK2 siRNA. The normalized C/Y emission ratio was quantified as a function of time after the addition of PZ09 (5 μM). Data are means ± SE from n ≥ 20 cells. (**D**) HeLa cells were first cotransfected with aCKAR and control siRNA (Control) or both SphK1 siRNA and SphK2 siRNA (SphK1/2). Where indicated in the legend, cells were then loaded with 1 μM caged S1P for 30 min, washed of extracellular caged S1P, exposed to UV light, incubated for another 5 min after photolysis (+hν), and, lastly, treated with DMSO vehicle or 5 μM PZ09 to measure basal activity. The normalized C/Y emission ratio was quantified as a function of time after DMSO or PZ09 treatment. Data are means ± SE from n ≥ 57 cells. (**E**) HeLa cells were transfected with aCKAR, then exposed to vehicle or loaded with 1 μM caged S1P for 30 min, washed of extracellular caged S1P, and pretreated with 10 μM VPC23019 for 5 min before live-cell imaging. Cells were then photolyzed to detect intracellular S1P-induced activation of endogenous aPKC and, lastly, treated with 5 μM PZ09. The normalized C/Y emission ratio was quantified as a function of time after photolysis. Data are means ± SE from n ≥ 37 cells. (**F**) mRNA expression of *S1PR1*, *S1PR2*, *S1PR3*, *S1PR4*, and *S1PR5* in HeLa cells were analyzed by RT-qPCR and normalized to that of glyceraldehyde 3-phosphate dehydrogenase (*GAPDH*). Data are means ± SE from at least three independent experiments. (**G**) HeLa cells were transfected with aCKAR and then pretreated with or without 10 μM VPC23019 (VPC) for 5 min before live-cell imaging. Cells were then stimulated with DMSO vehicle or S1P (100 nM or 10 μM, as indicated) during live-cell imaging and, lastly, treated with 5 μM PZ09. The normalized C/Y emission ratio was quantified as a function of time after photolysis. Data are means ± SE from n ≥ 16 cells.
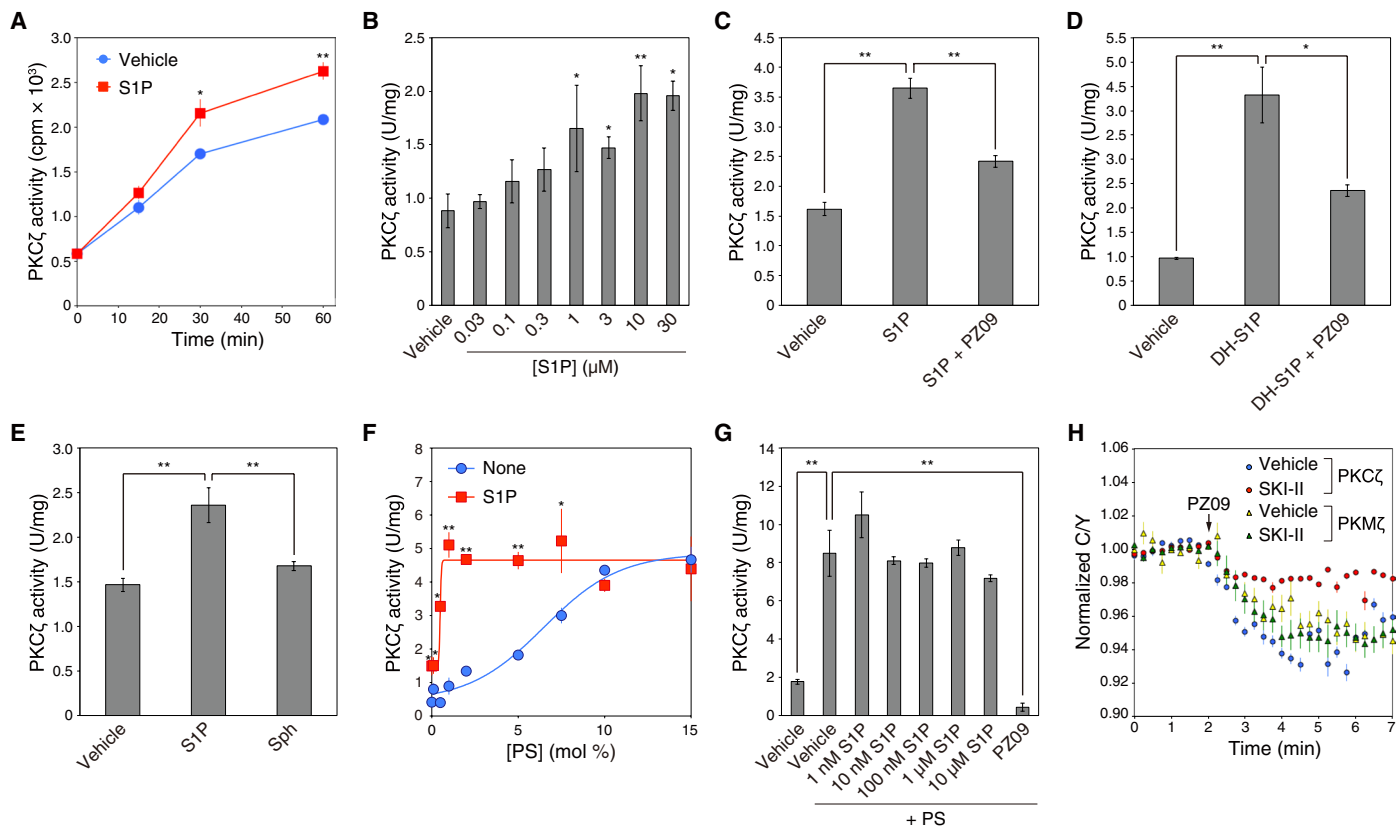
Fig. 4. Direct activation of aPKC by S1P. (**A**) Effect of S1P on activation of PKCζ assessed by an in vitro kinase assay. Kinase activity of purified GST (glutathione S-transferase)–PKCζ was measured in the absence (Vehicle) or presence of 30 μM S1P at the indicated time points. Data are means ± SE from at least three independent experiments. *$P < 0.05$ and **$P < 0.01$ versus vehicle at the same time point by Student's *t* test. (**B**) Dose-dependent effects of S1P on activation of PKCζ assessed by an in vitro kinase assay. Kinase activity of purified GST-PKCζ was measured for 60 min in the absence or presence of the indicated concentrations of S1P. Data are means ± SE from at least three independent experiments. *$P < 0.05$ and **$P < 0.01$ versus vehicle. (**C**) Kinase activity of purified GST-PKCζ was measured in the absence or presence of 30 μM S1P or 30 μM S1P + 10 μM PZ09. Data are means ± SE from at least three independent experiments. **$P < 0.01$. (**D**) Kinase activity of purified GST-PKCζ was measured in the absence or presence of 30 μM DH-S1P or 30 μM DH-S1P + 10 μM PZ09. Data are means ± SE from at least three independent experiments. *$P < 0.05$ and **$P < 0.01$. (**E**) Kinase activity of purified GST-PKCζ was measured in the absence or presence of 30 μM S1P or 30 μM Sph. Data are means ± SE from at least three independent experiments. **$P < 0.01$. (**F**) Kinase activity of purified GST-PKCζ was measured in the presence of Triton X-100 mixed micelles containing 0 to 15 mol % PS and 0 or 5 mol % S1P. Data are means ± SE from three independent experiments. *$P < 0.05$ and **$P < 0.01$. (**G**) Kinase activity of purified GST-PKCζ was measured in the absence or presence of PS (140 μM) with various concentrations of S1P or 10 μM PZ09. Data are means ± SE from at least three independent experiments. **$P < 0.01$. (**H**) HeLa cells were cotransfected with CKAR and mCherry-PKCζ or mCherry-PKMζ. Cells were pretreated with DMSO vehicle or 5 μM SKI-II for 16 hours and then treated with 5 μM PZ09. The normalized C/Y emission ratio was quantified as a function of time after PZ09 treatment. Data are means ± SE from $n ≥ 25$ cells.

involving in silico prediction and experimental validation (Fig. 6A). First, we constructed a homology model of the PKCζ kinase domain based on the crystal structure of PKCι (*44*) and used the Schrödinger's SiteMap algorithm (*45, 46*) to screen the surface of the kinase for possible binding sites. This model identified five potential binding pockets on PKCζ (Fig. 6B). Of these five potential sites, pocket 5 was the adenosine 5′-triphosphate (ATP)–binding site; therefore, only pockets 1, 2, 3, and 4 were selected for docking analysis. Induced fit docking (Schrödinger) (*47–49*), which accounts for the flexibility of the kinase, predicted the most energetically favorable docking pose for either S1P or Sph in each of these four potential binding pockets. S1P and Sph did not dock to pocket 4, and thus no binding scores were generated. The lowest docking scores of S1P to binding sites 1, 2, and 3 were −7.335, −7.753, and −8.583 kcal/mol, respectively (Fig. 6C). In comparison, the lowest docking scores of Sph to binding sites 1, 2, and 3 were −7.066, −6.586, and −7.424 kcal/mol,

respectively (Fig. 6C). In pocket 1, only one score was lower than −6.500 kcal/mol, whereas in pockets 2 and 3, several scores were lower than this threshold. In addition, in pockets 2 and 3, the docking scores for S1P were consistently better than the docking scores for Sph. These features make pockets 2 and 3 promising candidates for S1P-specific binding. From these data, we determined the binding poses for pockets 1, 2, and 3 with the most favorable docking scores (Fig. 6D) and the two-dimensional interaction diagrams (Fig. 6E). A similar result was obtained for S1P-PKCι binding (fig. S3). From these poses, we identified the following basic amino acid residues, lysine (Lys; K in the figure) and arginine (Arg; R in the figure), predicted to interact with S1P: Lys[265], Lys[284], and Arg[325] in pocket 1; Arg[375] and Lys[399] in pocket 2; and Lys[513] in pocket 3. We then mutated these basic residues in full-length PKCζ to neutral glutamine (Gln; Q in the figure) and monitored the effect of these mutations on S1P-induced activity in live cells. Pocket 1 mutation and
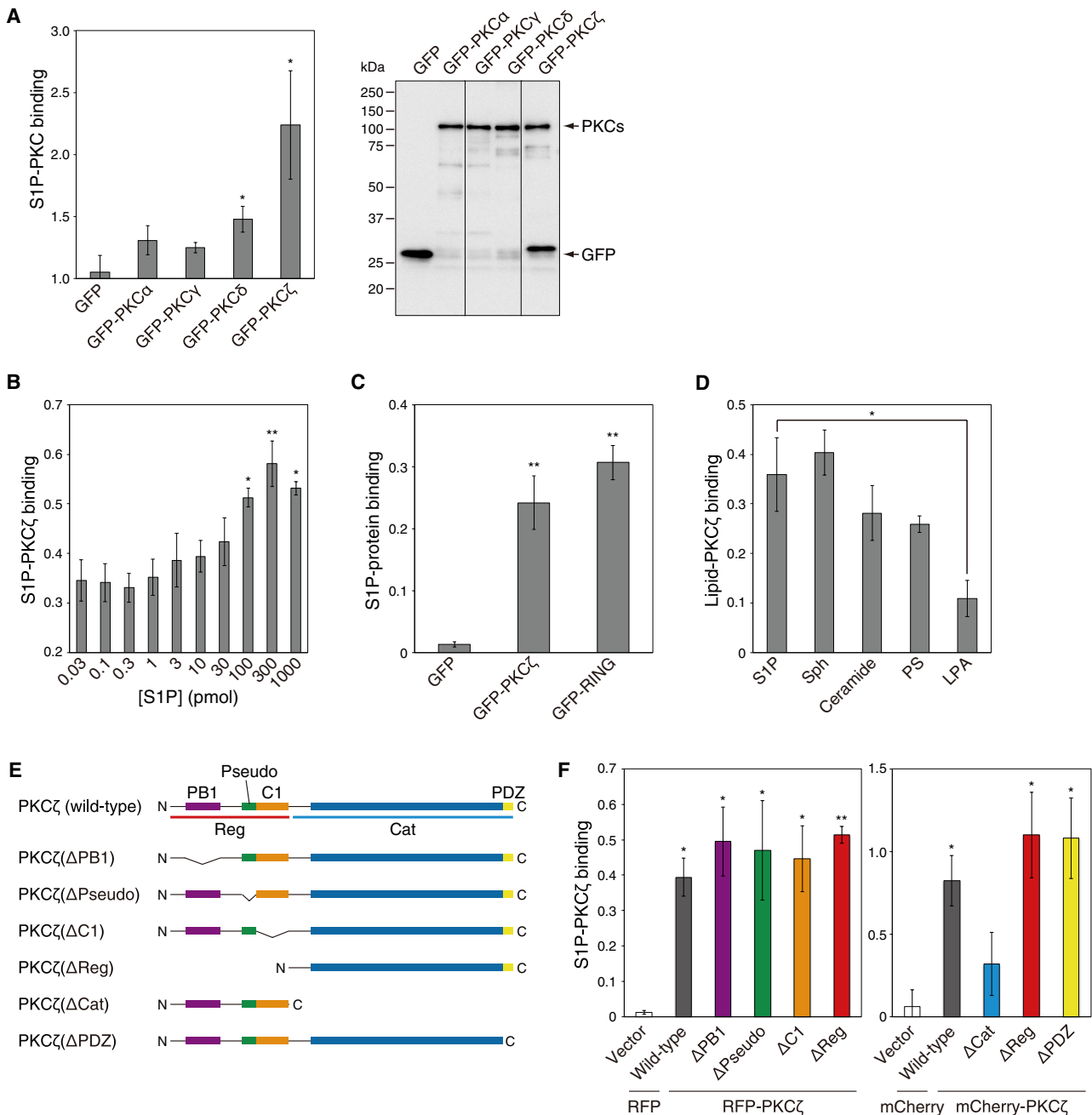
Fig. 5. Direct binding of S1P to aPKC. (**A**) COS7 cells were transfected with green-fluorescent protein (GFP), GFP-PKCα, GFP-PKCγ, GFP-PKCδ, or GFP-PKCζ. Left: S1P-PKC binding ability was measured by a protein-lipid binding assay with NBD-labeled S1P. Data are means ± SE from at least three independent experiments (*$P < 0.05$ versus GFP vector control). Right: Immunoprecipitated GFP or GFP-PKC was run on SDS–polyacrylamide gel electrophoresis (SDS-PAGE), and the amount of exogenously expressed GFP or GFP-PKC was detected via Western blot analysis using an anti-GFP antibody. (**B**) The binding affinity of PKCζ for S1P was assessed using the PLO assay. The interactions between purified GST-PKCζ and various concentrations of S1P were detected using an anti-GST antibody. Data are means ± SE from at least three independent experiments. *$P < 0.05$ and **$P < 0.01$ versus 0.03 pmol of S1P by Student's t test. (**C**) The binding affinity of PKCζ or the RING domain of TRAF2 for S1P was assessed by a PLO assay. The interaction between GFP, GFP-PKCζ, or GFP-tagged RING domain of TRAF2 (GFP-RING) and 30 pmol of S1P was detected using an anti-GST antibody. Data are means ± SE from at least three independent experiments. **$P < 0.05$ versus GFP vector control. (**D**) The binding affinity of PKCζ for related lipids was assessed by the PLO assay. The interactions between purified GST-PKCζ and 30 pmol of S1P, Sph, C16-ceramide (Ceramide), PS, or LPA were detected using an anti-GST antibody. Data are means ± SE from at least three independent experiments. *$P < 0.05$. (**E**) Domain schematic of deletion mutants of PKCζ. Structures of full-length PKCζ and six deletion mutants are shown. PB1, PB1 domain; Pseudo, pseudosubstrate segment; C1, C1 domain; PDZ, PDZ domain; Reg, regulatory domain; Cat, catalytic domain; N, N terminus; C, C terminus. (**F**) The binding affinity of domain deletion mutants of PKCζ for S1P was assessed using the PLO assay. The interactions between RFP- or mCherry-fused full-length PKCζ [RFP-PKCζ (wild-type) or mCherry-PKCζ (wild-type)], PB1 deletion mutant (ΔPB1), pseudosubstrate deletion mutant (ΔPseudo), C1 deletion mutant (ΔC1), regulatory domain deletion mutant (ΔReg) (PKMζ), catalytic domain deletion mutant (ΔCat), or PDZ deletion mutant (ΔPDZ) and 30 pmol of S1P were detected using an anti-GST antibody. The S1P-PKCζ binding affinity was compared to the RFP or mCherry vector control. Data are means ± SE from at least three independent experiments. *$P < 0.05$ and **$P < 0.01$ versus vector control.

Fig. 6. Identification of critical sites and amino acids for binding of aPKC to S1P. (**A**) Flow-chart of the strategy for identifying the critical sites and amino acids of PKCζ for S1P binding and S1P-induced activation is shown. The blue boxes indicate in silico assays, and the red boxes indicate cellular assays. (**B**) Potential ligand-binding pockets on the surface of the homology model of the catalytic domain of PKCζ predicted using the Schrödinger's SiteMap algorithm. (**C**) S1P or Sph was docked to the center of mass position for pocket 1, pocket 2, or pocket 3 on the catalytic domain of PKCζ using the induced fit docking protocol in the Schrödinger package. The five lowest docking scores from the induced fit docking for each pocket are shown in the bar graph (kcal/mol). IFD, induced fit docking. (**D**) The induced fit docking poses of S1P (carbon atoms in pink) to pocket 1, pocket 2, and pocket 3 of the catalytic domain of human PKCζ are shown with corresponding docking scores. These docking poses have the lowest dock-ing score (kcal/mol) in each pocket. (**E**) Two-dimensional interaction diagram of the S1P-PKCζ binding as in (D). Negatively charged, positively charged, polar, hydrophobic, and glycine resi-dues at the active site are represented by red, purple, cyan, green, and white spheres, respec-tively. Hydrogen bonds between the S1P and backbone or side chains are shown in solid pink arrows or dashed pink arrows, respectively. Salt bridges are shown in red-blue lines. Lys[82], Lys[101], and Arg[142] in pocket 1 correspond to Lys[265], Lys[284], and Arg[325] of full-length PKCζ. Arg[192] and Lys[216] in pocket 2 correspond to Arg[375] and Lys[399] of full-length PKCζ. Lys[330] in pocket 3 corresponds to Lys[513] of full-length PKCζ. (**F**) HeLa cells were cotransfected with aCKAR and mCherry (vector), mCherry-PKCζ (wild-type), mCherry-PKCζ(K265Q/K284Q/R325Q) (mutant for pocket 1; Pocket1mt), mCherry-PKCζ(R375Q/K399Q) (mutant for pocket 2; Pocket2mt), or mCherry-PKCζ(K513Q) (mutant for pocket 3; Pocket3mt). Cells were then loaded with 1 μM caged S1P for 30 min, washed, and pretreated with 10 μM VPC23019 for 5 min before live-cell imaging. Cells were photolyzed to detect intracellular S1P-induced activation of exogenous mCherry-PKCζ. The normalized C/Y emission ratio was quantified as a function of time after photolysis. Data are means ± SE from n ≥ 27 cells. (**G**) As in (F), except HeLa cells were cotransfected with aCKAR and mCherry (Vector), mCherry-PKCζ (Wild-type), mCherry-PKCζ(R375Q/K399Q) (Pocket2mt), mCherry-PKCζ(R375Q), or mCherry-PKCζ(K399Q) mutant. Data are means ± SE from n ≥ 17 cells. (**H**) Kinase activity of purified GST-PKCζ (Wild-type) or GST-PKCζ(R375Q/K399Q) (Pocket2mt)

was measured in the absence or presence of 30 μM S1P or 140 μM PS. Data are means ± SE from at least three independent experiments. *P < 0.05 by Student's t test. (**I**) HeLa cells were cotransfected with aCKAR and mCherry-PKCζ (Wild-type; left) or mCherry-PKCζ(R375Q/K399Q) (Pocket2mt; right). Cells were then pretreated with DMSO vehicle, 20 μM LY294002, or 5 μM SKI-II for 16 hours and then treated with 5 μM PZ09 during live-cell imaging to detect basal activity of exogenous mCherry-PKCζ. The normalized C/Y emission ratio was quantified as a function of time after PZ09 treatment. Data are means ± SE from n ≥ 25 cells. (**J**) HeLa cells were cotransfected with CKAR-PB1[Par6] and mCherry (Vector), mCherry-PKCζ (Wild-type), or mCherry-PKCζ(R375Q/K399Q) (Pocket2mt). Cells were then treated with 5 μM PZ09 during live-cell imaging to detect basal activity of exogenous mCherry-PKCζ. The normalized C/Y emission ratio was quantified as a function of time after PZ09 treatment. Data are means ± SE from n ≥ 16 cells.
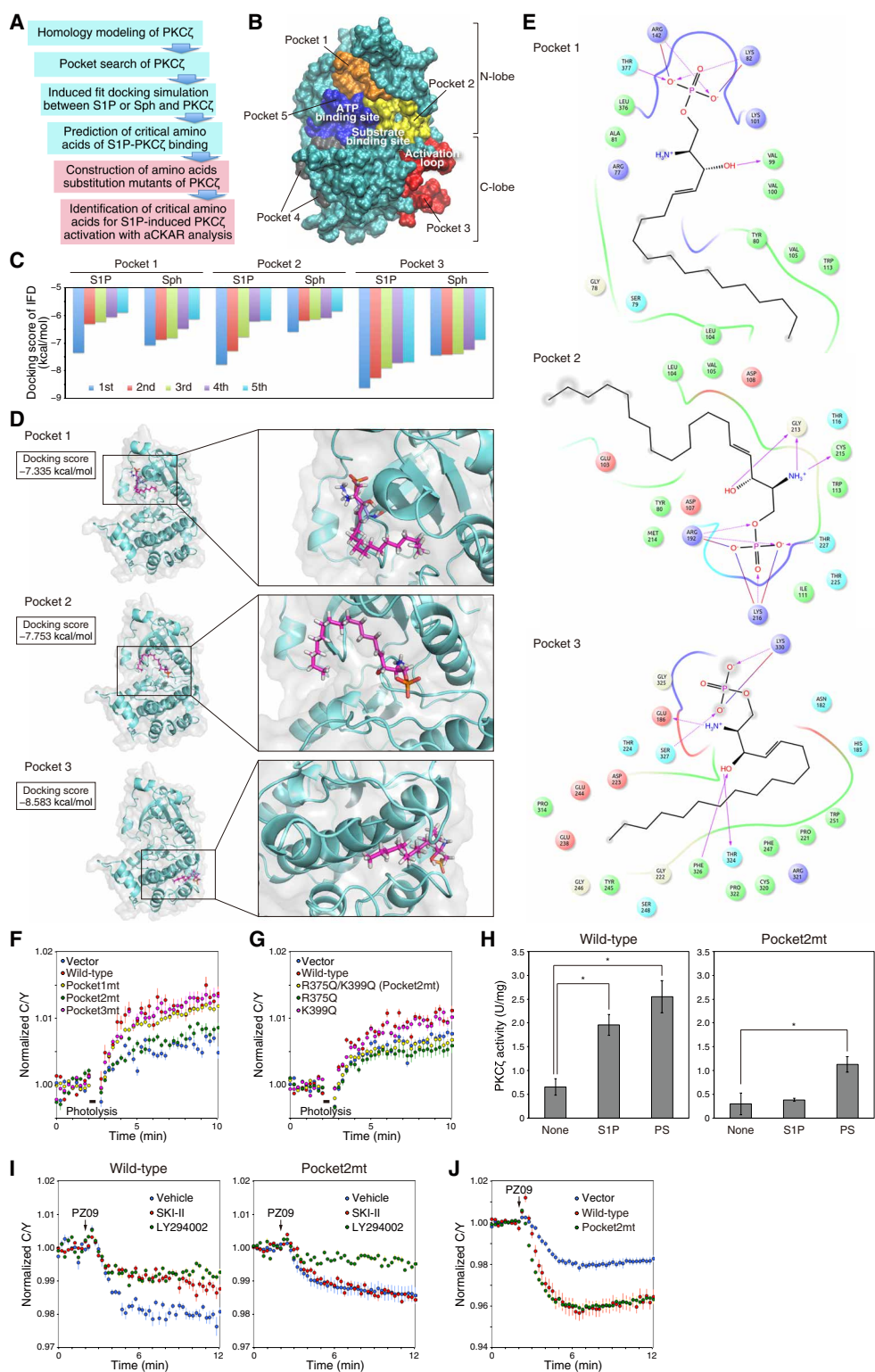
the pocket 3 mutation resulted in activation similar to that of wild-type PKCζ (yellow, pink, and red, respectively; Fig. 6F). However, the mutation of the residues in pocket 2 abolished activation above that seen endogenously (green and blue, Fig. 6F). Of the two residues predicted to interact with S1P in pocket 2, Arg[375] is the most critical: The single mutation R375Q (Fig. 6G, green), but not K399Q (pink), abolished the S1P-dependent activation of overexpressed PKCζ analogously to R375Q/R399Q (Fig. 6G, yellow). These data identify binding pocket 2 as an allosteric binding site that promotes S1P-dependent activation of PKCζ in cells. To validate that this is the site responsible for the S1P-induced activation of pure enzyme, we purified the PKCζ R375Q/R399Q mutant and examined its stimulation by S1P compared with that by PS. Concentrations of S1P that resulted in near maximal activation of wild-type PKCζ had no effect on the activity of the R375Q/R399Q mutant (Fig. 6H). The PS-dependent activity of this mutant was about half that of wild-type enzyme under the conditions of the assay, likely reflecting mutation of Arg[375], which is part of a conserved HRD motif in protein kinases (50); Gln is found at this position in some kinases (51). Nonetheless, the mutant had sufficient activity to establish that it was no longer sensitive to S1P. To confirm that this binding pocket was driving basal activation of aPKC by basal S1P, we examined how a mutation at this site affected SKI-II–sensitive signaling. SKI-II pretreatment had no effect on PZ09-mediated inhibition of PKCζ activity for the pocket 2 mutant (Fig. 6I, right, red), whereas it reduced the PZ09-mediated inhibition of wild-type PKCζ (Fig. 6I, left, red). As a control, the pocket 2 mutant had the same sensitivity to PI3K inhibition (Fig. 6I, green) as the wild-type enzyme. Thus, basic amino acid mutation of pocket 2 specifically prevented the activation of aPKC by basal S1P. Last, we found that the PKCζ R375Q/R399Q mutant had activity similar to wild-type enzyme on the Par6 scaffold (Fig. 6J). Although the mutation decreased the V_{max} (maximal velocity of the enzyme) twofold in vitro, its activity in a cellular context was similar to that of wild-type enzyme, likely because the CKAR readout is saturated in overexpression studies.

S1P-mediated activation of aPKC protects cells from apoptosis

We next addressed the physiological function for S1P-mediated activation of PKCζ; specifically, we explored whether S1P-dependent activation of PKCζ regulated apoptosis or necrosis. Treating HeLa cells (grown in 10% serum) with inhibitors of either SphK (SKI-II) or PI3K (LY294002) alone had no statistically significant effect on the number of apoptotic or necrotic cells, as assessed by staining with Apopxin Green (which detects exposed PS) and 7-aminoactinomycin D (7-AAD; a fluorescent DNA intercalator), respectively; however, inhibiting both SphK and PI3K did significantly increase the number of apoptotic, but not necrotic, cells (Fig. 7, A and B). The inhibition of aPKC with PZ09 also increased apoptosis (Fig. 7, A and B), suggesting that the effects of SKI-II and LY294002 could be mediated by inhibition of aPKC. We also investigated chromatin condensation, which correlates with apoptotic morphology (52), in HeLa cells with Hoechst 33342 staining and obtained similar results using PS exposure as a measure of apoptosis (Fig. 7C and fig. S4A). To examine the contribution of S1P in the absence of PI3K effects (Fig. 2F), serum-starved cells were treated with SKI-II. In the absence of serum, SKI-II treatment caused a statistically significant increase in the proportion of apoptotic and DNA-condensed cells (Fig. 7, D to F, and fig. S4B). Thus, under conditions of serum starvation, inhibition of SphK promotes apoptosis.

To dissect out the specific contribution of aPKC activation by S1P in suppressing apoptosis, we asked whether SKI-II–induced apoptosis could be rescued by constitutively active PKMζ. SKI-II treatment induced apoptosis in cells overexpressing PKCζ but was ineffective in inducing apoptosis in cells overexpressing PKMζ, whereas combined SKI-II and PZ09 treatment did (Fig. 7, G to I, and fig. S4C). The sensitivity of PKCζ-overexpressing cells, but not PKMζ-overexpressing cells, to SKI-II–induced apoptosis is consistent with basal S1P-induced activation of aPKC through relief of autoinhibition to suppress apoptosis. To validate the role of the S1P binding site in the cellular function of aPKC, we used siRNA to deplete both PKCζ and PKCι from HeLa cells. Knockdown of both aPKC isozymes caused a 10-fold increase in the proportion of apoptotic cells (Fig. 7, J and K). Overexpression of mCherry-tagged wild-type PKCζ in PKCζ/ι-depleted cells reduced the proportion of knockdown-induced apoptotic cells by a third, whereas overexpression of the mCherry-tagged R375Q/R399Q mutant did not (Fig. 7, J and K). These results are consistent with a model whereby aPKC suppresses apoptosis through a mechanism that depends on its ability to bind S1P.

DISCUSSION

In this study, we identified intracellular S1P as a lipid second messenger that allosterically activates aPKC isozymes. Using a genetically encoded activity reporter that we developed specifically for aPKC in cells, we found that (i) intracellular S1P enables signaling of aPKC and (ii) photolytic release of S1P from a caged lipid probe results in aPKC activation. This S1P-dependent activation of aPKC is not due to S1P receptor activation by extracellular S1P. Rather, it results from direct binding of intracellular S1P to the kinase domain, an event that relieves autoinhibitory constraints. Using molecular docking simulations, we identified a conserved S1P binding pocket on the kinase domains of PKCζ and PKCι/λ, which we validated biochemically. Lastly, cellular studies revealed that inhibition of SphK increased apoptosis in cells overexpressing PKCζ but not PKMζ, an alternative splice variant that lacks autoinhibitory constraints. These data are consistent with a model in which S1P binds the kinase domain of aPKC isozymes to partially activate these kinases, with this enhanced activity contributing to the suppression of apoptosis. Thus, S1P is a lipid mediator that promotes aPKC function.

The lack of small molecules to modulate aPKC activity in cells has made identifying substrates, measuring cellular activity, and determining signaling pathways considerably more challenging than for the diacylglycerol-dependent isozymes. For the latter, phorbol esters, functional analogs of diacylglycerol, revolutionized the study of the conventional and novel PKC isozymes by providing a tool to acutely activate these enzymes (53). The development and validation of a small-molecule inhibitor, PZ09, provided the first tool to successfully interrogate aPKC signaling in cells (12, 33, 54). However, the lack of specific agonists for aPKC activation has made it challenging to use existing pan-PKC reporters for PKC activity, such as CKAR (29), which reports on the activity of all PKC isozymes (31). Here, we engineered CKAR to specifically interrogate the spatiotemporal dynamics of aPKC signaling. This reporter, aCKAR, measures aPKC activity but not the activity of other PKC isozymes nor does it report the activity of the related AGC kinases AKT or PKA. The combination of a reporter tailored for aPKC and an aPKC-selective inhibitor allowed us not only to assess the basal activity of

Fig. 7. S1P-induced basal activity of aPKC is involved in apoptosis resistance. (**A**) HeLa cells were treated with DMSO vehicle, 5 μM SKI-II, 20 μM LY294002 (singly or combined), or 5 μM PZ09 for 12 hours. Cells were then stained with Hoechst 33342, Apopxin Green (Apoptosis), and 7-AAD (Necrosis) and observed by fluorescence microscopy. Scale bar, 20 μm. (**B**) Percentage of the Apopxin Green+ or 7-AAD+ cells was quantified respectively from the results represented in (A). Data are means ± SE from at least three independent experiments. **$P < 0.01$ versus vehicle by Student's t test. (**C**) HeLa cells were treated with the agents described in (A) for 24 hours. DNA condensation was then observed using Hoechst 33342 staining under fluorescence microscopy, and the percentage of condensed cells was quantified. Data are means ± SE from at least three independent experiments. **$P < 0.01$ versus vehicle. (**D**) HeLa cells were treated with DMSO vehicle or 5 μM SKI-II in the presence or absence of serum for 12 hours. Cells were then stained with Hoechst 33342, Apopxin Green, and 7-AAD and then observed by fluorescence microscopy. Scale bar, 20 μm. (**E**) Percentage of the Apopxin Green+ or 7-AAD+ cells was quantified respectively from the results in (D). Data are means ± SE from at least three independent experiments. *$P < 0.05$ and **$P < 0.01$. (**F**) HeLa cells were treated with DMSO vehicle or 5 μM SKI-II in the presence or absence of serum for 24 hours. DNA condensation was observed using Hoechst 33342 staining under fluorescence microscopy, and the percentage of condensed cells was quantified. Data are means ± SE from at least three independent experiments. *$P < 0.05$ and **$P < 0.01$. (**G**) HeLa cells were transfected with mCherry vector, mCherry-PKCζ, or mCherry-PKMζ. Cells were treated with DMSO vehicle, 5 μM SKI-II, or 5 μM SKI-II + 5 μM PZ09 in serum-free conditions for 12 hours, then stained with Apopxin Green, and observed by fluorescence microscopy. Arrows indicate costained cells. Scale bar, 20 μm. (**H**) Percentage of the Apopxin Green+ cells within the population of

mCherry+ cells was quantified from the results in (G). Data are means ± SE from at least three independent experiments. *$P < 0.05$ and **$P < 0.01$. (**I**) HeLa cells were transfected with mCherry vector, mCherry-PKCζ, or mCherry-PKMζ. Cells were treated as described in (G) for 24 hours. DNA condensation was observed using Hoechst 33342 staining under fluorescence microscopy, and the percentage of condensed cells was quantified. Data are means ± SE from at least three independent experiments. *$P < 0.05$ and **$P < 0.01$. (**J**) HeLa cells were cotransfected with control siRNA or both PKCζ siRNA and PKCι siRNA and mCherry (vector), mCherry-PKCζ, or mCherry-PKCζ(R375Q/K399Q). Cells were then serum-starved with serum-free medium for 12 hours. Cells were stained with Apopxin Green and then observed using fluorescence microscopy. Arrows indicate costained cells. Scale bar, 20 μm. (**K**) Percentage of the Apopxin Green+ cells within the population of mCherry+ cells was quantified from the results in (J). Data are means ± SE from at least three independent experiments. **$P < 0.01$. (**L**) Model depicting the proposed mechanism of S1P-mediated activation of aPKC that promotes a basal signaling output that suppresses apoptosis. aPKC is autoinhibited by interaction of the pseudosubstrate (Pseudo) with the substrate-binding cavity of the kinase domain (blue circle, top left). S1P, constitutively produced from Sph by SphK, binds to a pocket with basic amino acids (++), Arg375 and Lys399, close to the substrate-binding site in the kinase domain; this interaction displaces the pseudosubstrate to allow substrate binding and downstream signaling. This S1P-induced basal activation of aPKC promotes resistance to apoptosis. P, phosphate; ADP, adenosine 5′-diphosphate.
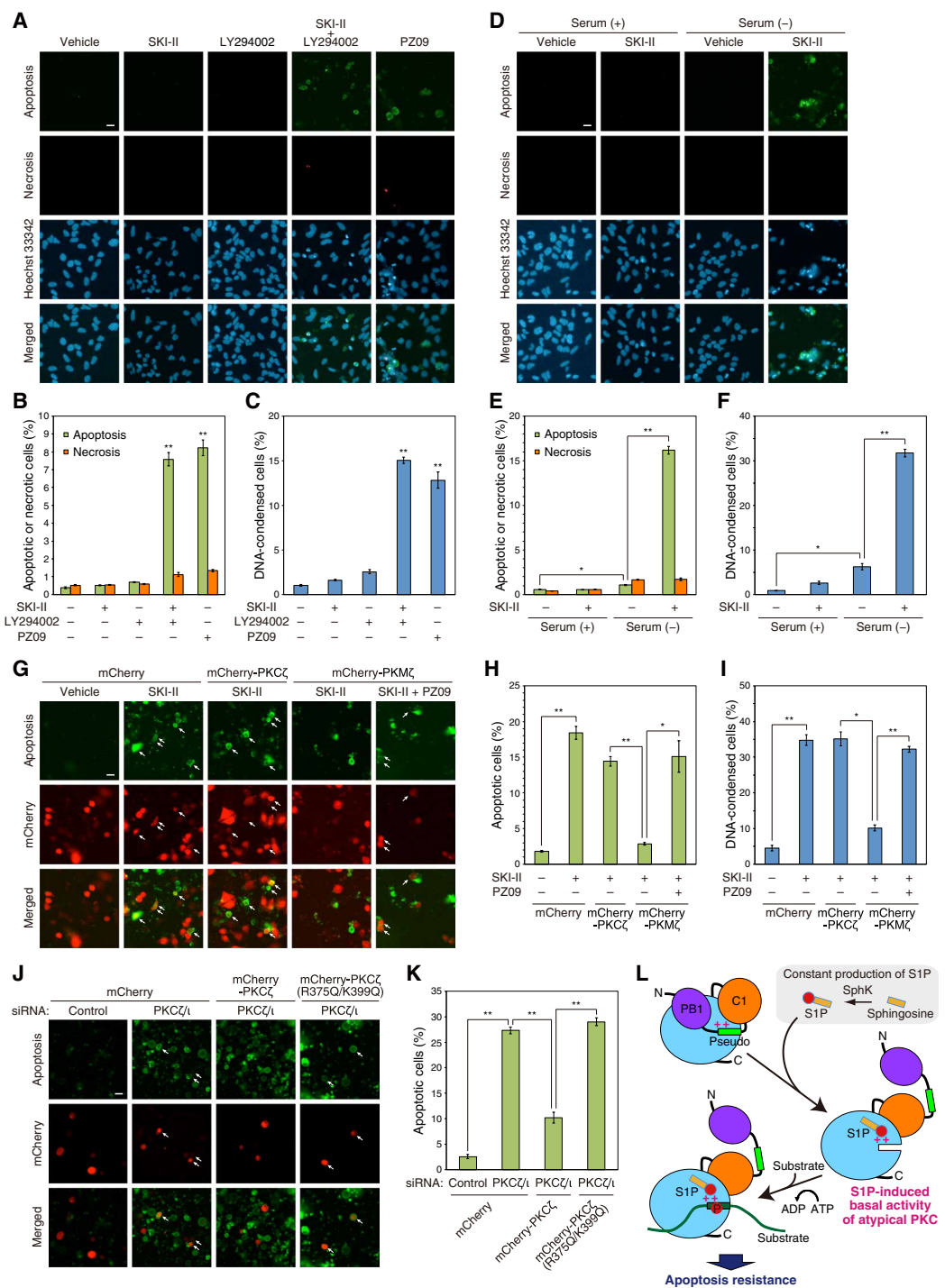
aPKC isozymes in a panel of cell lines but also to examine activation mechanisms of aPKC in cells. We found that basal aPKC activity was highest in the more aggressive breast cancer cell line MDA-MB-231 compared to the less aggressive MCF7 cell line and lowest in the liver cell line HepG2 and the neuroblastoma cell line SH-SY5Y. Thereafter, using live-cell imaging analysis of HeLa cells, which display readily detectable basal activity, we identified intracellular S1P as an activator of aPKC isozymes. This lipid mediator accounted for a substantial fraction of the basal activity of aPKC isozymes, with basal signaling by PI3K accounting for the remainder. Basally active aPKC was further stimulated by an acute increase of S1P abundance, as revealed by photolytic release of this lipid from caged S1P. Biochemical studies revealed that S1P directly bound the kinase domain of aPKC, thereby relieving autoinhibitory constraints. In addition, it decreased the concentration of PS necessary to half-maximally activate pure aPKC. Whereas ceramide has been previously reported to activate aPKC (13, 15, 55), the mechanism we report here is highly specific for S1P, which binds to a unique and defined pocket in the kinase domain to facilitate the release of autoinhibition.

As is the case for all PKC isozymes, aPKC isozymes are maintained in an autoinhibited conformation by interaction of a pseudosubstrate segment in the substrate-binding cavity (Fig. 7L, top left). Mechanisms that break intramolecular contacts of the pseudosubstrate result in substrate binding and downstream signaling. Whereas conventional and novel PKC isozymes are activated by binding the second messenger diacylglycerol, aPKC isozymes are activated by binding protein scaffolds through their PB1 domain. However, whether or not there are second messengers that contribute to release of the aPKC pseudosubstrate has remained unclear. Here, we show that S1P binds to a basic pocket on the surface of aPKC isozymes, disrupting autoinhibitory constraints (Fig. 7L, middle right) to allow substrate phosphorylation (Fig. 7L, bottom left). Thus, our findings reveal that S1P is an allosteric activator of aPKC isozymes. Consistent with S1P facilitating pseudosubstrate release and accompanying activation, Par6-bound aPKC was insensitive to S1P; this is expected given that aPKC bound to this scaffold is already in an open and active conformation (11, 12). Whether scaffolded aPKC dynamically exchanges with the cytosolic pool, and whether localized pools of S1P drive localized aPKC signaling, remains to be determined. That aside, at least one functional effect of S1P-induced activation of aPKC was suppression of apoptosis.

The ability of S1P to suppress apoptosis is consistent with the mounting body of literature establishing S1P as a mediator of survival signaling and SphK as an oncogene (17). Clinical data reveal that in renal and breast cancers, high amounts of SphK are associated with poor patient outcome (23, 56). Of the two aPKC isozymes, PKCι/λ serves as an oncogene in diverse cancers and diverse contexts (5). Although a number of loss-of-function mutations have been identified in cancers for both aPKC isozymes (4), our data reveal one context in which aPKC signaling is oncogenic. Our data identify an axis between oncogenic S1P signaling and oncogenic aPKC signaling.

The activation of aPKC isozymes by S1P unveils a context in which these isozymes may function as oncoproteins. Although the cancer-associated mutations in PKCζ and PKCι/λ that have been characterized to date are loss of function (suggesting a tumor suppressive role), considerable evidence supports an oncogenic function for these isozymes in certain contexts (57–60). Two particular

cancers in which PKCι/λ may be oncogenic are those of the lung and of the brain. In lung cancer, Fields and co-workers (61, 62) have identified a role for PKCι/λ in phosphorylating sex-determining region Y-box 2, a master transcriptional regulator of stemness. This isozyme is also tumor-initiating in K-RAS–mediated lung adeno-carcinomas by phosphorylating E74-like ETS transcription factor 3 (ELF-3) to control Notch expression (61). In patients with glioblastoma, high immunoreactivity for aPKC (primarily for PKCι/λ) correlates with poor disease prognosis; furthermore, an aPKC inhibitor reduces tumor growth in a mouse model of glioblastoma (54). In contrast, aPKC isozymes may function as tumor suppressors in other cancers. Loss of PKCζ in intestinal cells promotes metabolic reprogramming associated with a cancer phenotype (63, 64), and loss of PKCι/λ is observed in the intestinal epithelium of patients with Crohn's disease, a pathology associated with a high risk of cancer (65). Furthermore, mice lacking PKCι/λ in their intestinal epithelium have increased inflammation and tumorigenesis (65). Given that aPKC isozymes may function as both tumor suppressors and oncoproteins depending on the context, the link to S1P signaling suggests that patients with oncogenic SphK mutations may benefit from inhibition of aPKC signaling.

MATERIALS AND METHODS
Chemicals and antibodies
PDBu, forskolin, calyculin A, and LY294002 were purchased from Calbiochem. EGF was purchased from Upstate Biotechnology. PZ09 was obtained from Reagency. SKI-II, LPA, and cOmplete Mini Protease Inhibitor Cocktail were purchased from Sigma-Aldrich. Caged S1P was purchased from Santa Cruz Biotechnology. VPC23019 was purchased from Cayman Chemical. S1P, DH-S1P, Sph, and C16-ceramide were purchased from Enzo Life Sciences. NBD-labeled S1P and PS were purchased from Avanti Polar Lipids. The anti-PKCζ antibody was purchased from Santa Cruz Biotechnology (C-20, SC-216). The anti-PKCι antibody was purchased from BD (clone 23, 610176). The anti–β-actin antibody was purchased from Sigma-Aldrich (clone AC-74, A2228). The anti-GFP (clone mFX75, 012-22541) and anti-GST (clone 5A7, 013-21851) antibodies were purchased from Wako Pure Chemical Industries. All other materials were reagent grade.

Plasmid constructs and mutagenesis
AKAR was a gift from R. Tsien, University of California, San Diego (UCSD) (34). CKAR, BKAR, DKAR, and CKAR-PB1^{Par6} were described previously (12, 29, 35, 36). aCKAR was generated through substitution of an aPKC substrate sequence, AKLLGMTFMIRSSG, for the substrate sequence within CKAR. The phosphoacceptor Thr was mutated to an alanine to create aCKAR-T/A using the QuikChange mutagenesis protocol (Stratagene). Human PKCζ, human PKMζ, human PKCζ(ΔPDZ) (residues 1 to 589 of human PKCζ), human PKCα, rat PKCβII, human PKCδ, human PKCε, mouse Akt1, and human PKD1 constructs were amplified and cloned into the pDONR221 vector; these were then recombined with various pDEST vectors constructed in-house to make fusion proteins with an N-terminal mCherry tag in pcDNA3 for mammalian cell expression or an N-terminal GST tag in a pFastBac backbone vector for insect cell expression using the Gateway cloning system (Invitrogen) (9, 12, 66, 67). mCherry-PKCζ(ΔCat) was made by removing the residues from 184 to 592 of full-length

mCherry-PKCζ. Rat PKCζ, rat PKMζ, or mouse PKCλ (residues 136 to 595 of mouse PKCλ) was amplified and cloned into an N-terminal monomeric RFP (mRFP)–tagged pcDNA3 vector for making RFP-PKCζ, RFP-PKMζ, or RFP catalytic domain of PKCλ [RFP-PKCλ(Cat)]. RFP-PKCζ(ΔPB1), RFP-PKCζ(ΔPseudo), or RFP-PKCζ(ΔC1) was made by removing the residues from 25 to 106 for ΔPB1, from 113 to 130 for ΔPS, or from 131 to 183 for ΔC1 of full-length RFP-rat PKCζ, respectively. mCherry-PKCζ(ΔPB1) was made by removing the residues from 25 to 106 of full-length mCherry-PKCζ. For mCherry-PKCζ(K265Q/K284Q/R325Q), mCherry-PKCζ(R375Q/K399Q), mCherry-PKCζ(K513Q), mCherry-PKCζ(R375Q), and mCherry-PKCζ(K399Q), lysine or arginine was mutated to a glutamine using the QuikChange mutagenesis protocol. GFP-PKCα, GFP-PKCγ, GFP-PKCδ, and GFP-PKCζ were provided by N. Saito (Kobe University). The RING domain of human TRAF2 (residues 28 to 101) was amplified and cloned into pmCherry-N1 (Clontech) for making GFP-RING domain of TRAF2.

Short interfering RNAs
For RNA interference, we used the following siRNAs: for hPKCζ (forward: 5′-CGUGAUUGACCCUUUAACUdGdT-3′; reverse: 5′-AGUUAAAGGGUCAAUCACGdCdG-3′; dX is deoxyribosylthymine throughout), for hPKCι (forward: 5′-GUACUGUUG-GUUCGAUUAAdAdA-3′; reverse: 5′-UUAAUCGAACCAA-CAGUACdTdT-3′), for hSphK1 (forward: 5′-GGGCAAGGCCUU-GCAGCUCdTdT-3′; reverse: 5′-GAGCUGCAAGGCCUUGC-CCdTdT-3′), for hSphK2 (forward: 5′-GCUGGGCUGUCCUU-CAACCUdTdT-3′; reverse: 5′-AGGUUGAAGGACAGCCCAGC-dTdT-3′), and for nontargeting control (forward: 5′-GGGCAAGG-CUCUGAAGCUCdTdT-3′; reverse: 5′-GAGCUUCAGAGCCU-UGCCCdTdT-3′). The target sequence of the hPKCζ siRNA is in 3′ untranslated region of hPKCζ mRNA, and those of the other siRNAs, aside from the nontargeting control, are in the coding region of each respective mRNA. The siRNAs for hPKCζ and hPKCι were synthesized by Dharmacon, and the siRNAs for control, hSphK1, and hSphK2 were synthesized by Japan Bio Services.

Cell culture and transfection
COS7, HEK293, MCF7, MDA-MB-231, and SH-SY5Y cells were purchased from American Type Culture Collection. HeLa cells were a gift from N. Saito (Kobe University). HepG2 cells were a gift from J. Olefsky (UCSD). Cells were maintained in Dulbecco's modified Eagle's medium (Mediatech) containing 10% fetal bovine serum and 1% penicillin/streptomycin at 37°C in 5% CO$_2$. Cells were plated onto sterilized plastic culture plates or glass-bottom 35-mm culture dishes before transfection. Transient transfection was carried out using FuGENE HD (Promega), and all experiments were performed 2 to 3 days after the transfection. In case of knockdown experiments, transient transfection of siRNAs or both siRNAs and plasmids was carried out using Lipofectamine 2000 (Thermo Fisher Scientific), and all experiments were performed 48 hours after the transfection.

FRET imaging
Cells expressing kinase activity reporters were rinsed once with and imaged in Hank's balanced salt solution containing 1 mM CaCl$_2$. Images were acquired on a Zeiss Axiovert microscope (Carl Zeiss) using a MicroMax digital camera (Roper Industries) controlled by MetaFluor software (Universal Imaging). Optical filters were obtained from Chroma Technology. Using a 10% neutral density filter,

CFP and FRET images were obtained every 15 s using a 420/20-nm excitation filter, a 450-nm dichroic mirror, and a 475/40-nm emission filter (CFP) or 535/25-nm emission filter (FRET). YFP emission was also monitored as a control for photobleaching through a 495/10-nm excitation filter, a 505-nm dichroic mirror, and a 535/25-nm emission filter. Excitation and emission filters were switched in filter wheels (Lambda 10-2, Sutter Instrument). Integration times were 200 ms for CFP and FRET and 100 ms for YFP. RFP (or mCherry) images were obtained through a 568/55-nm excitation filter, a 600-nm dichroic mirror, and a 653/95-nm emission filter. Images were reanalyzed using MetaFluor Analyst (Universal Imaging). One region per cell was selected such that there was no net movement of the targeted reporter in and out of the selected region, and MetaFluor Analyst was used to calculate the average FRET ratio within the selected region. The trace for each cell imaged was normalized to its $t = 0$ to 2 min averaging baseline value. The normalized C/Y emission ratios were combined from three independent experiments and represented as the average of these corrected values ±SE.

Loading of caged S1P
HeLa cells grown on glass-bottom culture dishes were preloaded with 1 μM caged S1P for 30 min. After washing out the media, dishes were then flashed with UV light (254 nm) for 30 s from 5-cm distance for photolysis of caged S1P.

Real-time quantitative reverse transcription PCR
Total RNA was extracted from HeLa cells (2 × 10⁶ cells) using NucleoSpin RNA II (Macherey-Nagel) according to the manufacturer's instructions. Reverse transcription was carried out using 1 μg of RNA (ReverTra Ace qPCR RT kit, Toyobo). RT-qPCR was performed with SYBR Premix (Takara Bio) on ABI Prism 7000 (Applied Biosystems). The primer sequences (sense and antisense) were as follows: for human S1P$_1$ (*S1PR1*) (forward: 5′-TTCCTGGTGT-TAGCTGTGCTCAAC-3′; reverse: 5′-TCGCTTGAATTTGC-CAGCAGAGTC-3′), for human S1P$_2$ (*S1PR2*) (forward: 5′-TGCG-CCATTGTGGTGGAAAACC-3′; reverse: 5′-TTGCCCAGAAA-CAGGTACATTGCC-3′), for human S1P$_3$ (*S1PR3*) (forward: 5′-AGCAGCAACAATAGCAGCCACTC-3′; reverse: 5′-AGT-GCTGCGTTCTTGTCCATGATG-3′), for human S1P$_4$ (*S1PR4*) (forward: 5′-AACTGCCTGTGCGCCTTTGAC-3′; reverse: 5′-AT-CACCAGGCAGAAGAGGATGTAGC-3′), for human S1P$_5$ (*S1PR5*) (forward: 5′-TTCCTGCTGCTGTTGCTCGAC-3′; reverse: 5′-TTCAGAAGTGAGTTGGCCATGGC-3′), for human SphK1 (*SPHK1*) (forward: 5′-AGCTTCCTTGAACCATTAT-GCTG-3′; reverse: 5′-AGGTCTTCATTGGTGACCTGCT-3′), for human SphK2 (*SPHK2*) (5′-ATGAATGGACACCTTGAAG-CAG-3′; reverse: 5′-CATGGCCTTAGCCCTGACCAG-3′), for human *GAPDH* (forward: 5′-GCCATCAATGACCCCTTCATT-3′; reverse: 5′-TCTCGCTCCTGGAAGATGG-3′). The expression of each mRNA was normalized to *GAPDH* mRNA expression.

Purification of GST-PKC
Baculoviruses were made in High Five or SF9 insect cells from pFastBac plasmids using the Bac-to-Bac expression system (Invitrogen). Batch purification using glutathione resin beads (Novagen) was used to purify the GST-tagged proteins from infected High Five or SF9 insect cell cultures. Briefly, cells were rinsed with phosphate-buffered saline (PBS) and lysed in 50 mM Hepes (pH 7.5), 100 mM NaCl, and 1 mM dithiothreitol (DTT) (buffer A) with 0.1% Triton X-100, 100 μM

phenylmethylsulfonyl fluoride (PMSF), 2 mM benzamidine, and leupeptin (50 µg/ml). The soluble lysate was incubated with glutathione resin beads for 30 min at 4°C. Protein-bound beads were washed three times in buffer A and then eluted three times in buffer A with 10 mM glutathione. Eluent was loaded in a 30-kDa Amicon Ultra centrifugal filter unit (Millipore) and washed or concentrated three times with buffer B [20 mM Hepes (pH 7.5) and 1 mM DTT]. Glycerol was added to 50% volume before measurement of GST-PKCζ concentration using bovine serum albumin standards on a Coomassie brilliant blue stained gel, and enzyme stocks were stored at −20°C.

In vitro kinase activity assay

PKC activity was assayed by measuring the incorporation of $^{32}P_i$ from [γ-^{32}P]ATP into substrate as described previously (9, 68). Kinase activity was measured in 80-µl reactions supplemented with PS, S1P, or Sph at the concentrations indicated in figure legends. In some experiments, Triton X-100/lipid mixed micelles containing 0 to 15 mol % PS and 0 or 5 mol % of S1P in 1% Triton X-100 (Thermo Fisher Scientific) were made, as described previously (41), and diluted 10 times in the reaction mixture. The reaction mixture contained 20 mM Hepes (pH 7.4), 5 mM MgCl₂, 100 µM ATP, [γ-^{32}P]ATP (10 µCi/ml) (PerkinElmer), MBP (50 µg/ml; Sigma-Aldrich), 30 ng of purified GST-PKCζ, and the lipids indicated in the figure legends. The incubation was carried out for indicated times at 30°C. Reactions were stopped by addition of 25 mM ATP and 25 mM EDTA (pH 8.0) and spotted on pieces of P81 Whatman cellulose phosphate filter paper. Filter papers were washed four times with 0.4% phosphoric acid before measurement using a scintillation counter (Beckman).

Western blots

Cells were harvested with lysis buffer [50 mM Na₂HPO₄, 1 mM sodium pyrophosphate, 20 mM NaF, 2 mM EDTA, 2 mM EGTA, 1% Triton X-100, 1 mM DTT, 200 µM benzamidine, leupeptin (40 µg/ml), and 1 mM PMSF]. The detergent-solubilized cell lysate was obtained by centrifuging the whole-cell lysate in a microcentrifuge at 13,000 rpm for 5 min. The detergent-solubilized lysates were separated on a 7.5% SDS-PAGE gel, blotted onto polyvinylidene difluoride membrane (Bio-Rad), and probed with an anti-PKCζ antibody (diluted 1:1000), anti-PKCι antibody (diluted 1:1000), or anti–β-actin antibody (diluted 1:1000), followed by incubation with horseradish peroxidase (HRP)–conjugated secondary antibodies and further imaging using enhanced chemiluminescence with SuperSignal West Pico Chemiluminescent Substrate (Thermo Fisher Scientific). Images were acquired using FluorChem Q (Alpha Innotech). For the S1P-PKC binding assay, immunoprecipitated GFP or GFP-PKC bound with NBD-S1P samples were detergent-solubilized and separated on a 10% SDS-PAGE gel, blotted onto polyvinylidene difluoride membrane (Millipore), and probed with an anti-GFP antibody (diluted 1:1000). HRP-conjugated secondary antibody labeling of blots was detected using enhanced chemiluminescence with SuperSignal West Dura Extended Duration Substrate (Thermo Fisher Scientific). Images were acquired using LAS3000 (Fujifilm). Quantification of Western blots was performed using ImageJ software [National Institutes of Health (NIH)].

In vitro PKC-S1P binding assay

COS7 cells transfected with empty vector, GFP, GFP-PKCα, GFP-PKCγ, GFP-PKCδ, or GFP-PKCζ were harvested and lysed in lysis buffer [10 mM tris-HCl (pH 7.6), 150 mM NaCl, and 0.05% Tween 20 with cOmplete Mini Protease Inhibitor Cocktail], sonicated on ice, and centrifuged at 10,000g for 30 min at 4°C, and the supernatant was collected. GFP or GFP-PKC was immunoprecipitated using anti-GFP antibody affinity agarose beads (Nacalai Tesque), and immunoprecipitates were washed with PBS. The immunoprecipitated GFP or GFP-PKC isozymes were mixed with 0.4 µg of NBD-S1P and rotated for 24 hours at 4°C. After washing the beads by centrifugation, PKC bound to NBD-S1P was isolated using a chloroform/methanol method described previously (69). The aldehyde/sulfate latex beads (4×10^4) were added, and the mixture was rotated overnight at 4°C. After washing the beads, NBD-S1P fluorescence on the aldehyde/sulfate latex beads was detected using FACSCalibur (BD) with an excitation wavelength of 488 nm. Total fluorescence intensity of NBD-S1P on aldehyde/sulfate latex beads was calculated and normalized with that of aldehyde/sulfate latex beads only. Last, the S1P-PKC binding unit was calculated by ratio of none to GFP or none to GFP-PKC isozymes.

PLO assay

Purified GST-PKCζ (500 ng/ml) was used to probe bovine serum albumin–blocked nitrocellulose filters (Echelon Research Laboratories) on which various phospholipids had been spotted. The filters were washed, and GST-PKCζ bound to the filters was immunostained with anti-GST antibody (Amersham Biosciences) and anti-mouse immunoglobulin G (Alexa Fluor 488 conjugate, Cell Signaling Technology) secondary antibody and then fluorescently detected using an EnSpire Multimode Plate Reader (PerkinElmer). For mammalian cell–expressed PKC, COS7 cells transfected with RFP-PKC or mCherry-PKC were harvested in lysis buffer [10 mM tris-HCl (pH 7.6), 150 mM NaCl, and 0.05% Tween 20 with cOmplete Mini Protease Inhibitor Cocktail], sonicated on ice, and centrifuged at 10,000g for 30 min to collect supernatant. The cell lysates containing RFP-PKC or mCherry-PKC were applied to the S1P-spotted filters and allowed to incubate for 1 hour at room temperature, filters were then washed, and the fluorescence of RFP or mCherry on the filter was detected using an EnSpire Multimode Plate Reader. The fluorescence intensity of S1P-bound RFP-PKC or mCherry-PKC on the filter was normalized to the fluorescence intensity of RFP-PKC or mCherry-PKC in the cell lysate.

Induced fit docking simulation

The crystal structure of PKCι (Protein Data Bank: 4 DC2) determined at a 2.40-Å resolution was used to construct a homology model of human PKMζ (NM_001033581) and 232 to 596 amino acids of human PKCι (NM_002740) using the SWISS-MODEL server (https://swissmodel.expasy.org) (70). The surface of the homology model of human PKCζ or human PKCι was screened for potential binding sites with Schrödinger's SiteMap (Schrödinger Release 2016-1: SiteMap, Schrödinger LLC) (45, 46). S1P and Sph were prepared by LigPrep in the Schrödinger package using default parameters (Schrödinger Release 2016-1: LigPrep, Schrödinger LLC). These ligands were docked to the center of mass position of each identified site (1 to 5) using the induced fit docking protocol in Schrödinger (Schrödinger Release 2016-1: Schrödinger Suite 2016-1 Induced Fit Docking protocol; Glide, Schrödinger, LLC; Prime, Schrödinger LLC) (47–49). The five lowest-energy docking poses were further evaluated. The resulting model skeleton structures of the poses of S1P or Sph binding to PKCζ or PKCι were observed

and analyzed using PyMOL software (MacPyMOL: PyMOL v1.8.6.0 enhanced for Mac OS X, Schrödinger LLC).

Chromatin condensation assay

After various treatments for 24 hours, both attached and floating HeLa cells were collected in PBS, followed by staining for DNA using NucBlue Live ReadyProbes Reagent (Thermo Fisher Scientific). Images of the fluorescence of Hoechst 33342 dye were obtained under a Zeiss Axiovert fluorescence microscope. The number of cells showing chromatin changes with two or more condensed chromatin fragments in their nuclei was manually counted using ImageJ software (NIH).

Apoptosis versus necrosis detection assay

HeLa cells were treated with various treatments for 12 hours, and the cells were stained with the Apoptosis/Necrosis Detection Kit (Abcam) according to the manufacturer's instructions. Images of Apoxin Green and 7-AAD were obtained under a Zeiss Axiovert fluorescence microscope. The cells stained with Apoxin Green were counted as early stages of apoptotic cells, and the cells labeled with 7-AAD were counted as necrotic cells using ImageJ software (NIH).

Quantification and statistical analyses

All statistical data are presented as means ± SE. The statistical significance of differences was determined with Student's t test using GraphPad Prism 6 (GraphPad Software). $P < 0.05$ was considered to be statistically significant.

SUPPLEMENTARY MATERIALS

www.sciencesignaling.org/cgi/content/full/12/562/eaat6662/DC1
Fig. S1. Phosphatase sensitivity of aCKAR is greater than that of CKAR.
Fig. S2. S1P signaling does not affect the Par6-regulated basal activity of PKCζ in breast cancer cells.
Fig. S3. Identification of critical sites and amino acids for PKCι-S1P binding in silico.
Fig. S4. Apoptotic nuclear morphology images.

REFERENCES AND NOTES

1. M. L. Drummond, K. E. Prehoda, Molecular control of atypical protein kinase C: Tipping the balance between self-renewal and differentiation. *J. Mol. Biol.* **428**, 1455–1464 (2016).
2. A. Suzuki, S. Ohno, The PAR-aPKC system: Lessons in polarity. *J. Cell Sci.* **119**, 979–987 (2006).
3. M. T. Diaz-Meco, J. Moscat, The atypical PKCs in inflammation: NF-κB and beyond. *Immunol. Rev.* **246**, 154–167 (2012).
4. A. C. Newton, J. Brognard, Reversing the paradigm: Protein kinase C as a tumor suppressor. *Trends Pharmacol. Sci.* **38**, 438–447 (2017).
5. P. J. Parker, V. Justilien, P. Riou, M. Linch, A. P. Fields, Atypical protein kinase Cι as a human oncogene and therapeutic target. *Biochem. Pharmacol.* **88**, 1–11 (2014).
6. J. Qian, P. P. Massion, Role of chromosome 3q amplification in lung cancer. *J. Thorac. Oncol.* **3**, 212–215 (2008).
7. A. C. Newton, Protein kinase C as a tumor suppressor. *Semin. Cancer Biol.* **48**, 18–26 (2018).
8. J. A. Le Good, W. H. Ziegler, D. B. Parekh, D. R. Alessi, P. Cohen, P. J. Parker, Protein kinase C isotypes controlled by phosphoinositide 3-kinase through the protein kinase PDK1. *Science* **281**, 2042–2045 (1998).
9. I. S. Tobias, M. Kaulich, P. K. Kim, N. Simon, E. Jacinto, S. F. Dowdy, C. C. King, A. C. Newton, Protein kinase Cζ exhibits constitutive phosphorylation and phosphatidylinositol-3,4,5-triphosphate-independent regulation. *Biochem. J.* **473**, 509–523 (2016).
10. L.-C. L. Tsai, L. Xie, K. Dore, L. Xie, J. C. Del Rio, C. C. King, G. Martinez-Ariza, C. Hulme, R. Malinow, P. E. Bourne, A. C. Newton, Zeta inhibitory peptide disrupts electrostatic interactions that maintain atypical protein kinase C in its active conformation on the scaffold p62. *J. Biol. Chem.* **290**, 21845–21856 (2015).
11. C. Graybill, B. Wee, S. X. Atwood, K. E. Prehoda, Partitioning-defective protein 6 (par-6) activates atypical protein kinase C (aPKC) by pseudosubstrate displacement. *J. Biol. Chem.* **287**, 21003–21011 (2012).
12. I. S. Tobias, A. C. Newton, Protein scaffolds control localized protein kinase Cζ activity. *J. Biol. Chem.* **291**, 13809–13822 (2016).
13. N. A. Bourbon, J. Yun, M. Kester, Ceramide directly activates protein kinase C ζ to regulate a stress-activated protein kinase signaling complex. *J. Biol. Chem.* **275**, 35617–35623 (2000).
14. T. E. Fox, K. L. Houck, S. M. O'Neill, M. Nagarajan, T. C. Stover, P. T. Pomianowski, O. Unal, J. K. Yun, S. J. Naides, M. Kester, Ceramide recruits and activates protein kinase C ζ (PKCζ) within structured membrane microdomains. *J. Biol. Chem.* **282**, 12450–12457 (2007).
15. G. Wang, K. Krishnamurthy, N. S. Umapathy, A. D. Verin, E. Bieberich, The carboxyl-terminal domain of atypical protein kinase Cζ binds to ceramide and regulates junction formation in epithelial cells. *J. Biol. Chem.* **284**, 14469–14475 (2009).
16. G. Wang, J. Silva, K. Krishnamurthy, E. Tran, B. G. Condie, E. Bieberich, Direct binding to ceramide activates protein kinase Cζ before the formation of a pro-apoptotic complex with PAR-4 in differentiating stem cells. *J. Biol. Chem.* **280**, 26415–26424 (2005).
17. Y. A. Hannun, L. M. Obeid, Sphingolipids and their metabolism in physiology and disease. *Nat. Rev. Mol. Cell Biol.* **19**, 175–191 (2018).
18. H. Le Stunff, S. Milstien, S. Spiegel, Generation and metabolism of bioactive sphingosine-1-phosphate. *J. Cell. Biochem.* **92**, 882–899 (2004).
19. M. Maceyka, K. B. Harikumar, S. Milstien, S. Spiegel, Sphingosine-1-phosphate signaling and its role in disease. *Trends Cell Biol.* **22**, 50–60 (2012).
20. K. Mendelson, T. Evans, T. Hla, Sphingosine 1-phosphate signalling. *Development* **141**, 5–9 (2014).
21. R. L. Proia, T. Hla, Emerging biology of sphingosine-1-phosphate: Its role in pathogenesis and therapy. *J. Clin. Invest.* **125**, 1379–1387 (2015).
22. G. M. Strub, M. Maceyka, N. C. Hait, S. Milstien, S. Spiegel, Extracellular and intracellular actions of sphingosine-1-phosphate. *Adv. Exp. Med. Biol.* **688**, 141–155 (2010).
23. K. Geffken, S. Spiegel, Sphingosine kinase 1 in breast cancer. *Adv. Biol. Regul.* **67**, 59–65 (2018).
24. N. J. Pyne, S. Pyne, Sphingosine 1-phosphate and cancer. *Nat. Rev. Cancer* **10**, 489–503 (2010).
25. P. Xia, J. R. Gamble, L. Wang, S. M. Pitson, P. A. B. Moretti, B. W. Wattenberg, R. J. D'Andrea, M. A. Vadas, An oncogenic role of sphingosine kinase. *Curr. Biol.* **10**, 1527–1530 (2000).
26. S. E. Alvarez, K. B. Harikumar, N. C. Hait, J. Allegood, G. M. Strub, E. Y. Kim, M. Maceyka, H. Jiang, C. Luo, T. Kordula, S. Milstien, S. Spiegel, Sphingosine-1-phosphate is a missing cofactor for the E3 ubiquitin ligase TRAF2. *Nature* **465**, 1084–1088 (2010).
27. N. C. Hait, J. Allegood, M. Maceyka, G. M. Strub, K. B. Harikumar, S. K. Singh, C. Luo, R. Marmorstein, T. Kordula, S. Milstien, S. Spiegel, Regulation of histone acetylation in the nucleus by sphingosine-1-phosphate. *Science* **325**, 1254–1257 (2009).
28. S. Panneer Selvam, R. M. De Palma, J. J. Oaks, N. Oleinik, Y. K. Peterson, R. V. Stahelin, E. Skordalakes, S. Ponnusamy, E. Garrett-Mayer, C. D. Smith, B. Ogretmen, Binding of the sphingolipid S1P to hTERT stabilizes telomerase at the nuclear periphery by allosterically mimicking protein phosphorylation. *Sci. Signal.* **8**, ra58 (2015).
29. J. D. Violin, J. Zhang, R. Y. Tsien, A. C. Newton, A genetically encoded fluorescent reporter reveals oscillatory phosphorylation by protein kinase C. *J. Cell Biol.* **161**, 899–909 (2003).
30. A. Mahajan, C. Yuan, H. Lee, E. S.-W. Chen, P.-Y. Wu, M.-D. Tsai, Structure and function of the phosphothreonine-specific FHA domain. *Sci. Signal.* **1**, re12 (2008).
31. T. Kajimoto, S. Sawamura, Y. Tohyama, Y. Mori, A. C. Newton, Protein kinase Cδ-specific activity reporter reveals agonist-evoked nuclear activity controlled by Src family of kinases. *J. Biol. Chem.* **285**, 41896–41910 (2010).
32. J. Ryu, J. S. Hah, J. S. S. Park, W. Lee, A. L. Rampal, C. Y. Jung, Protein kinase C-ζ phosphorylates insulin-responsive aminopeptidase in vitro at Ser-80 and Ser-91. *Arch. Biochem. Biophys.* **403**, 71–82 (2002).
33. J. I. Trujillo, J. R. Kiefer, W. Huang, A. Thorarensen, L. Xing, N. L. Caspers, J. E. Day, K. J. Mathis, K. K. Kretzmer, B. A. Reitz, R. A. Weinberg, R. A. Stegeman, A. Wrightstone, L. Christine, R. Compton, X. Li, 2-(6-phenyl-1*H*-indazol-3-yl)-1*H*-benzo[*d*]imidazoles: Design and synthesis of a potent and isoform selective PKC-ζ inhibitor. *Bioorg. Med. Chem. Lett.* **19**, 908–911 (2009).
34. J. Zhang, C. J. Hupfeld, S. S. Taylor, J. M. Olefsky, R. Y. Tsien, Insulin disrupts β-adrenergic signalling to protein kinase a in adipocytes. *Nature* **437**, 569–573 (2005).
35. M. T. Kunkel, Q. Ni, R. Y. Tsien, J. Zhang, A. C. Newton, Spatio-temporal dynamics of protein kinase B/Akt signaling revealed by a genetically encoded fluorescent reporter. *J. Biol. Chem.* **280**, 5581–5587 (2005).
36. M. T. Kunkel, A. Toker, R. Y. Tsien, A. C. Newton, Calcium-dependent regulation of protein kinase D revealed by a genetically encoded kinase activity reporter. *J. Biol. Chem.* **282**, 6733–6742 (2007).
37. K. J. French, R. S. Schrecengost, B. D. Lee, Y. Zhuang, S. N. Smith, J. L. Eberly, J. K. Yun, C. D. Smith, Discovery and evaluation of inhibitors of human sphingosine kinase. *Cancer Res.* **63**, 5962–5969 (2003).
38. T. Kajimoto, T. Okada, S. Miya, L. Zhang, S.-i. Nakamura, Ongoing activation of sphingosine 1-phosphate receptors mediates maturation of exosomal multivesicular endosomes. *Nat. Commun.* **4**, 2712 (2013).

39. P. V. Usatyuk, D. He, V. Bindokas, I. A. Gorshkova, E. V. Berdyshev, J. G. N. Garcia, V. Natarajan, Photolysis of caged sphingosine-1-phosphate induces barrier enhancement and intracellular activation of lung endothelial cell signaling pathways. *Am. J. Phys. Lung Cell. Mol. Phys.* **300**, L840–L850 (2011).

40. Y. A. Hannun, C. R. Loomis, R. M. Bell, Activation of protein kinase C by triton X-100 mixed micelles containing diacylglycerol and phosphatidylserine. *J. Biol. Chem.* **260**, 10039–10043 (1985).

41. J. W. Orr, A. C. Newton, Interaction of protein kinase C with phosphatidylserine. 1. Cooperativity in lipid binding. *Biochemistry* **31**, 4661–4667 (1992).

42. A. C. Newton, D. E. Koshland Jr., Phosphatidylserine affects specificity of protein kinase C substrate phosphorylation and autophosphorylation. *Biochemistry* **29**, 6656–6661 (1990).

43. J. A. Callender, A. C. Newton, Conventional protein kinase C in the brain: 40 years later. *Neuronal Signal.* **1**, NS20160005 (2017).

44. C. Wang, Y. Shang, J. Yu, M. Zhang, Substrate recognition mechanism of atypical protein kinase Cs revealed by the structure of PKCι in complex with a substrate peptide from par-3. *Structure* **20**, 791–801 (2012).

45. T. Halgren, New method for fast and accurate binding-site identification and analysis. *Chem. Biol. Drug Des.* **69**, 146–148 (2007).

46. T. A. Halgren, Identifying and characterizing binding sites and assessing druggability. *J. Chem. Inf. Model.* **49**, 377–389 (2009).

47. R. Farid, T. Day, R. A. Friesner, R. A. Pearlstein, New insights about HERG blockade obtained from protein modeling, potential energy mapping, and docking studies. *Bioorg. Med. Chem.* **14**, 3160–3173 (2006).

48. W. Sherman, T. Day, M. P. Jacobson, R. A. Friesner, R. Farid, Novel procedure for modeling ligand/receptor induced fit effects. *J. Med. Chem.* **49**, 534–553 (2006).

49. W. Sherman, H. S. Beard, R. Farid, Use of an induced fit receptor structure in virtual screening. *Chem. Biol. Drug Des.* **67**, 83–84 (2006).

50. S. S. Taylor, M. M. Keshwani, J. M. Steichen, A. P. Kornev, Evolution of the eukaryotic protein kinases as dynamic molecular switches. *Philos. Trans. R. Soc. Lond. B Biol. Sci.* **367**, 2517–2528 (2012).

51. D. I. McSkimming, S. Dastgheib, T. R. Baffi, D. P. Byrne, S. Ferries, S. T. Scott, A. C. Newton, C. E. Eyers, K. J. Kochut, P. A. Eyers, N. Kannan, KinView: A visual comparative sequence analysis tool for integrated kinome research. *Mol. Biosyst.* **12**, 3651–3665 (2016).

52. J. Yu, L. Zhang, P. M. Hwang, K. W. Kinzler, B. Vogelstein, PUMA induces the rapid apoptosis of colorectal cancer cells. *Mol. Cell* **7**, 673–682 (2001).

53. A. C. Newton, Protein kinase C: Poised to signal. *Am. J. Physiol. Endocrinol. Metab.* **298**, E395–E402 (2010).

54. Y. Kusne, E. A. Carrera-Silva, A. S. Perry, E. J. Rushing, E. K. Mandell, J. D. Dietrich, A. E. Errasti, D. Gibbs, M. E. Berens, J. C. Loftus, C. Hulme, W. Yang, Z. Lu, K. Aldape, N. Sanai, C. V. Rothlin, S. Ghosh, Targeting aPKC disables oncogenic signaling by both the EGFR and the proinflammatory cytokine TNFα in glioblastoma. *Sci. Signal.* **7**, ra75 (2014).

55. G. Müller, M. Ayoub, P. Storz, J. Rennecke, D. Fabbro, K. Pfizenmaier, PKC zeta is a molecular switch in signal transduction of TNF-alpha, bifunctionally regulated by ceramide and arachidonic acid. *EMBO J.* **14**, 1961–1969 (1995).

56. M. Uhlen, C. Zhang, S. Lee, E. Sjöstedt, L. Fagerberg, G. Bidkhori, R. Benfeitas, M. Arif, Z. Liu, F. Edfors, K. Sanli, K. von Feilitzen, P. Oksvold, E. Lundberg, S. Hober, P. Nilsson, J. Mattsson, J. M. Schwenk, H. Brunnström, B. Glimelius, T. Sjöblom, P. H. Edqvist, D. Djureinovic, P. Micke, C. Lindskog, A. Mardinoglu, F. Ponten, A pathology atlas of the human cancer transcriptome. *Science* **357**, eaan2507 (2017).

57. A. M. Butler, M. L. Scotti Buzhardt, S. Li, K. E. Smith, A. P. Fields, N. R. Murray, Protein kinase C zeta regulates human pancreatic cancer cell transformed growth and invasion through a STAT3-dependent mechanism. *PLOS ONE* **8**, e72061 (2013).

58. A. Paul, S. Gunewardena, S. R. Stecklein, B. Saha, N. Parelkar, M. Danley, G. Rajendran, P. Home, S. Ray, I. Jokar, G. A. Vielhauer, R. A. Jensen, O. Tawfik, S. Paul, PKCλ/ι signaling promotes triple-negative breast cancer growth and metastasis. *Cell Death Differ.* **21**, 1469–1481 (2014).

59. R. P. Regala, C. Weems, L. Jamieson, J. A. Copland, E. A. Thompson, A. P. Fields, Atypical protein kinase Cι plays a critical role in human lung cancer cell growth and tumorigenicity. *J. Biol. Chem.* **280**, 31109–31115 (2005).

60. A. J. Urtreger, M. G. Kazanietz, E. D. Bal de Kier Joffé, Contribution of individual PKC isoforms to breast cancer progression. *IUBMB Life* **64**, 18–26 (2012).

61. S. A. Ali, V. Justilien, L. Jamieson, N. R. Murray, A. P. Fields, Protein kinase Cι drives a NOTCH3-dependent stem-like phenotype in mutant *KRAS* lung adenocarcinoma. *Cancer Cell* **29**, 367–378 (2016).

62. V. Justilien, M. P. Walsh, S. A. Ali, E. A. Thompson, N. R. Murray, A. P. Fields, The *PRKCI* and *SOX2* oncogenes are co-amplified and cooperate to activate hedgehog signaling in lung squamous cell carcinoma. *Cancer Cell* **25**, 139–151 (2014).

63. V. Llado, Y. Nakanishi, A. Duran, M. Reina-Campos, P. M. Shelton, J. F. Linares, T. Yajima, A. Campos, P. Aza-Blanc, M. Leitges, M. T. Diaz-Meco, J. Moscat, Repression of intestinal stem cell function and tumorigenesis through direct phosphorylation of β-catenin and yap by PKCζ. *Cell Rep.* **10**, 740–754 (2015).

64. L. Ma, Y. Tao, A. Duran, V. Llado, A. Galvez, J. F. Barger, E. A. Castilla, J. Chen, T. Yajima, A. Porollo, M. Medvedovic, L. M. Brill, D. R. Plas, S. J. Riedl, M. Leitges, M. T. Diaz-Meco, A. D. Richardson, J. Moscat, Control of nutrient stress-induced metabolic reprogramming by PKCζ in tumorigenesis. *Cell* **152**, 599–611 (2013).

65. Y. Nakanishi, M. Reina-Campos, N. Nakanishi, V. Llado, L. Elmen, S. Peterson, A. Campos, S. K. De, M. Leitges, H. Ikeuchi, M. Pellecchia, R. S. Blumberg, M. T. Diaz-Meco, J. Moscat, Control of paneth cell fate, intestinal inflammation, and tumorigenesis by PKCλ/ι. *Cell Rep.* **16**, 3297–3310 (2016).

66. C. E. Antal, A. M. Hudson, E. Kang, C. Zanca, C. Wirth, N. L. Stephenson, E. W. Trotter, L. L. Gallegos, C. J. Miller, F. B. Furnari, T. Hunter, J. Brognard, A. C. Newton, Cancer-associated protein kinase C mutations reveal kinase's role as tumor suppressor. *Cell* **160**, 489–502 (2015).

67. D. Chen, A. Purohit, E. Halilovic, S. J. Doxsey, A. C. Newton, Centrosomal anchoring of protein kinase C βII by pericentrin controls microtubule organization, spindle function, and cytokinesis. *J. Biol. Chem.* **279**, 4829–4839 (2004).

68. T. Kajimoto, Y. Shirai, N. Sakai, T. Yamamoto, H. Matsuzaki, U. Kikkawa, N. Saito, Ceramide-induced apoptosis by translocation, phosphorylation, and activation of protein kinase Cδ in the Golgi complex. *J. Biol. Chem.* **279**, 12668–12676 (2004).

69. T. Fujita, T. Okada, S. Hayashi, S. Jahangeer, N. Miwa, S.-i. Nakamura, δ-Catenin/NPRAP (neural plakophilin-related armadillo repeat protein) interacts with and activates sphingosine kinase 1. *Biochem. J.* **382**, 717–723 (2004).

70. L. Bordoli, F. Kiefer, K. Arnold, P. Benkert, J. Battey, T. Schwede, Protein structure homology modeling using SWISS-MODEL workspace. *Nat. Protoc.* **4**, 1–13 (2009).

Science Signaling

Activation of atypical protein kinase C by sphingosine 1-phosphate revealed by an aPKC-specific activity reporter

Taketoshi Kajimoto, Alisha D. Caliman, Irene S. Tobias, Taro Okada, Caila A. Pilo, An-Angela N. Van, J. Andrew McCammon, Shun-ichi Nakamura and Alexandra C. Newton

Atypical activation of cell survival

The function and regulation of atypical protein kinase C (aPKC) isoforms are less well understood than those of the wider PKC family, and aPKCs are not activated by the same signals that activate conventional PKCs. Kajimoto *et al.* developed a live-cell imaging reporter to study aPKC activation mechanisms and discovered that basal pools of the lipid S1P bound to and activated aPKC by disrupting its autoinhibitory conformation. S1P-induced activation of aPKC suppressed apoptotic signals in various cell types. Given that both aPKC and S1P are individually associated with cancer, these findings reveal that the kinase and lipid are directly linked in a cell survival mechanism.

ARTICLE TOOLS	http://stke.sciencemag.org/content/12/562/eaat6662
SUPPLEMENTARY MATERIALS	http://stke.sciencemag.org/content/suppl/2018/12/20/12.562.eaat6662.DC1
RELATED CONTENT	http://stke.sciencemag.org/content/sigtrans/7/338/ra75.full http://stke.sciencemag.org/content/sigtrans/9/427/ra47.full
REFERENCES	This article cites 70 articles, 27 of which you can access for free http://stke.sciencemag.org/content/12/562/eaat6662#BIBL
PERMISSIONS	http://www.sciencemag.org/help/reprints-and-permissions

Use of this article is subject to the Terms of Service